# Oncostatin M triggers brain inflammation by compromising blood-brain barrier integrity

Peer-reviewed author version

HERMANS, Doryssa; HOUBEN, Evelien; BAETEN, Paulien; Slaets, Helena; JANSSENS, Kris; HOEKS, Cindy; HOSSEINKHANI, Baharak; DURAN, Gayel; BORMANS, Seppe; Gowing, Elizabeth; Hoornaert , Chloe; BECKERS, Lien; Fung, Wing Ka; Schroten, Horst; Ishikawa, Hiroshi; FRAUSSEN, Judith; THOELEN, Ronald; de Vries, Helga E.; Kooij, Gijs; Zandee, Stephanie; Prat, Alexandre; HELLINGS, Niels & BROUX, Bieke (2022) Oncostatin M triggers brain inflammation by compromising blood-brain barrier integrity. In: ACTA NEUROPATHOLOGICA, 144 (2), p. 259-281.

DOI: 10.1007/s00401-022-02445-0
Handle: http://hdl.handle.net/1942/37568

# Oncostatin M triggers brain inflammation by compromising blood-brain barrier integrity

Hermans Doryssa[1,2]*, Houben Evelien[1,2]*, Baeten Paulien[1,2], Slaets Helena[1,2], Janssens Kris[1,2], Hoeks Cindy[1,2], Hosseinkhani Baharak[1,2], Duran Gayel[1,2], Bormans Seppe[3], Gowing Elizabeth[4], Hoornaert Chloé[4], Beckers Lien[1,5], Fung Wing Ka[6], Schroten Horst[7], Ishikawa Hiroshi[8], Fraussen Judith[1,5], Thoelen Ronald[3], de Vries Helga E.[6], Kooij Gijs[6], Zandee Stephanie[4], Prat Alexandre[4], Hellings Niels[1,2]*, Broux Bieke[1,2,9]*

[1]University MS Center, Campus Diepenbeek, Diepenbeek, Belgium. [2]Neuro-Immune Connections and Repair Lab, Department of Immunology and Infection, Biomedical Research Institute, UHasselt, Diepenbeek, Belgium. [3]Institute for Materials Research (IMO), UHasselt, Diepenbeek, Belgium. [4]Neuroimmunology Unit, Centre de recherche du CHUM (CRCHUM), Montreal, Quebec, Canada. [5]Department of Immunology and Infection, Biomedical Research Institute, UHasselt, Diepenbeek, Belgium. [6]Amsterdam UMC, Vrije Universiteit Amsterdam, Department of Molecular Cell Biology and Immunology, Amsterdam Neuroscience, MS Center Amsterdam, Amsterdam, The Netherlands. [7]Pediatric Infectious Diseases, University Children's Hospital Mannheim, Medical Faculty Mannheim, Heidelberg University, Mannheim, Germany. [8]Laboratory of Clinical Regenerative Medicine, Department of Neurosurgery, Faculty of Medicine, University of Tsukuba, Japan. [9]Cardiovascular Research Institute Maastricht, Department of Internal Medicine, Maastricht University, Maastricht, The Netherlands.
*Equal contribution

## Abstract

Oncostatin M (OSM) is an IL-6 family member which exerts neuroprotective and remyelination-promoting effects after damage to the central nervous system (CNS). However, the role of OSM in neuro-inflammation is poorly understood. Here, we investigated OSM's role in pathological events important for the neuro-inflammatory disorder multiple sclerosis (MS). We show that OSM receptor (OSMRβ) expression is increased on circulating lymphocytes of MS patients, indicating their elevated responsiveness to OSM signalling. In addition, OSM production by activated myeloid cells and astrocytes is increased in MS brain lesions. In experimental autoimmune encephalomyelitis (EAE), a preclinical model of MS, OSMRβ-deficient mice exhibit milder clinical symptoms, accompanied by diminished T helper 17 (Th17) cell infiltration into the CNS and reduced BBB leakage. *In vitro*, OSM reduces BBB integrity by downregulating the junctional molecules claudin-5 and VE-cadherin, while promoting secretion of the Th17-attracting chemokine CCL20 by inflamed BBB-endothelial cells and reactive astrocytes. Using flow cytometric fluorescence resonance energy transfer (FRET) quantification, we found that OSM-induced endothelial CCL20 promotes activation of lymphocyte function-associated antigen 1 (LFA-1) on Th17 cells. Moreover, CCL20 enhances Th17 cell adhesion to OSM-treated inflamed endothelial cells, which is at least in part ICAM-1 mediated. Together, these data identify an OSM-CCL20 axis, in which OSM contributes significantly to BBB impairment during neuro-inflammation by inducing permeability while recruiting Th17 cells via enhanced endothelial CCL20 secretion and integrin activation. Therefore, care should be taken when considering OSM as a therapeutic agent for treatment of neuro-inflammatory diseases such as MS.

## Keywords

Oncostatin M; T helper 17 cells; Endothelial cells; Blood-brain barrier; Neuroinflammation; Multiple sclerosis

## Corresponding author

Bieke Broux, PhD

Bieke.broux@uhasselt.be

+3211269254

## Acknowledgements

This work was financially supported by grants from the Research Foundation of Flanders (FWO Vlaanderen, G097318N), and Bijzonder Onderzoeksfonds (BOF) UHasselt. The hCMEC/D3 cell line was provided by Tebu-bio (Le Perray-en-Yvelines, France). OSMRβ KO mice (B6.129S-Osmr <tm1Mtan>) were provided by the RIKEN BRC through the National Bio-Resource Project of MEXT, Japan. We would like to thank Lyne Bourbonnière for assistance in HBMEC culture, Dr. Antoine Fournier, Marc Charabati and Sam Duwé for technical assistance, and Britt Coenen, Athanasios Bethanis, Jules Teuwen, Ina Vantyghem and Kardelen Irem Isin for their practical help with experiments.

## Author contributions

Conceptualization: BB, NH; methodology: DH, EH, PB, HS, KJ, CH, BH, GD, SB, EG, ChH, LB, KFW, JF, SZ, RT, AP; formal analysis: DH, EH, CH, KJ, JF, SZ; writing-original draft: DH, EH, KJ; writing-review and editing: BB, NH, HS, GK, HEdV; visualization: DH; supervision: BB, NH. All authors have read and agreed to the published version of the manuscript.

## Conflict of interest

The authors declare that they have no conflict of interest.

## Introduction

To protect the brain's delicate microenvironment from pathogenic and inflammatory invaders, it is tightly regulated by the blood-brain barrier (BBB), a complex network of specialized endothelial cells (ECs), pericytes and the glia limitans. This establishes a physical barrier between the blood and central nervous system (CNS) parenchyma [38, 41]. Firmly connected ECs, mediated by adherens (AJs) and tight junctions (TJs), support low para- and transcellular transport of molecules across the BBB. In addition, cerebral ECs express low levels of cell adhesion molecules, such as intercellular (ICAM-1) and vascular cell adhesion molecule 1 (VCAM-1), reflecting the low level of immune surveillance in the healthy CNS [38, 41].

BBB impairment has been observed in various neuro-degenerative and -inflammatory disorders, such as multiple sclerosis (MS). Here, autoreactive T lymphocytes cross the BBB, causing local inflammation and CNS damage [12]. During this process of immune cell transmigration, BBB integrity becomes compromised due to the release of leukocyte-derived pro-inflammatory cytokines. This results in an altered localization and expression of TJs, cell adhesion molecule upregulation (e.g. ICAM-1, VCAM-1) and chemokine secretion (e.g. CCL2, CXCL10), making the BBB susceptible to further immune cell trafficking [38, 41]. A local exacerbated immune response ultimately leads to myelin breakdown and axonal damage. As demyelination continues, MS develops into a clinically apparent neurological disease including symptoms such as sensation deficits, and motor, autonomic and cognitive disabilities [12].

Levels of oncostatin M (OSM), a member of the IL-6 cytokine family, are increased in the blood and CNS of MS patients [16, 25, 53]. We previously identified that OSM has both neuroprotective and remyelinating properties [23]. More specifically, OSM limits neuronal excitotoxicity and promotes neurite outgrowth [44, 55, 68]. Moreover, we demonstrated that OSM signalling protects against demyelination and boosts remyelination in the cuprizone mouse model [24, 28]. Cytokines of the IL-6 family use the common receptor subunit glycoprotein 130 (gp130) which couples to its cytokine-specific receptor subunit. The latter is tightly regulated and restricts the amount of responding target cells [30, 47]. In humans, OSM exerts its effects through signaling via both the OSM receptor (OSMR; consisting of gp130 and OSMRβ) and leukemia inhibitory factor receptor (LIFR; consisting of gp130 and LIFRβ). In contrast, OSM does not signal through the LIFR in mice [9, 14, 23, 26, 36]. Overall, OSM is a promising therapeutic candidate to treat MS, since it could tackle the neuro-degenerative hallmark of the disease. However, the role of OSM in neuro-inflammation and more specifically at the level of the BBB, still remains elusive.

In the current study, we demonstrate that OSMR is highly upregulated on circulating lymphocytes in untreated MS patients, compared to healthy controls. In MS brain lesions, OSM is locally produced by macrophages/microglia and astrocytes. In mice with a constitutive knock-out (KO) of OSMRβ, experimental autoimmune encephalomyelitis (EAE) develops with milder disease symptoms, which is associated with diminished T helper 17 (Th17) cell infiltration into the CNS and reduced BBB leakage. Moreover, we found that OSM signalling impairs BBB integrity *in vitro* via downregulation of junctional molecules claudin-5 and VE-cadherin. While promoting CCL20 secretion by inflamed BBB-ECs and astrocytes, OSM, in contrast, reduces ICAM-1 and VCAM-1 expression on inflamed BBB-ECs. CCL20 in turn enhances Th17 cell adhesion by integrin $\alpha_L$

activation. In conclusion, we identify OSM as an inducer of BBB impairment and indirect recruiter of Th17 cells towards neuro-inflammatory sites.

## Material and Methods

### Study subjects

For characterization of OSMR expression on immune cells, peripheral blood samples from a previously collected cohort were used [29], including 22 healthy controls (HC), 41 untreated and 37 treated MS patients. Patients received treatment with IFN-β (Avonex®, Rebif®, Betaferon®), glatiramer acetate (Copaxone®) or Natalizumab (Tysabri®). Treated, untreated (at time of sampling) and healthy subjects were age- and sex-matched. Clinical data are summarized in Table 1. Blood samples were collected in collaboration with the University Biobank Limburg (UBiLim, Hasselt, Belgium). For immunohistochemistry, frozen brain material from 6 chronic progressive MS patients and 2 non-demented controls (NDC) without CNS inflammatory disease was obtained from the Netherlands Brain Bank (NBB, Amsterdam, Netherlands). Further clinical details are summarized in Table 2. This study was approved by the Medical Ethical Committee of Hasselt university and the University Hospital K.U.Leuven. Informed consent was obtained from all study subjects.

**Table 1** Study subjects used for analysis of the OSMR on circulating lymphocytes

| | **Treated MS patients** | **Untreated MS patients** | **Healthy controls** |
|---|---|---|---|
| *Number* | N = 37 | N = 41 | N = 22 |
| *Age (years)* | 43.68 | 46.63 | 39.59 |
| *Male/Female ratio* | 12/25 (0.48) | 13/28 (0.46) | 9/13 (0.69) |
| *Disease duration (years)* | 11.29 | 12.37 | NA |
| *EDSS* | 3.31 | 3.87 | NA |
| *MS type* | | | |
| - *Relapsing remitting* | 28 | 23 | NA |
| - *Chronic progressive* | 8 | 15 | NA |
| *Treatments* | | | |
| - *IFN-β* | 19 | NA | NA |
| - *Glatiramer acetate* | 7 | NA | NA |
| - *Natalizumab* | 11 | NA | NA |

EDSS, expanded disability status scale; IFN-β, interferon beta; NA, not applicable.

**Table 2** Study subjects used for brain tissue

| | **Age (years)** | **Sex** | **Lesion type** | **MS type** | **Cause of death** |
|---|---|---|---|---|---|
| *MS 1* | 64 | M | Active | Chronic progressive | Euthanasia |
| *MS 2* | 56 | F | Active | Chronic progressive | Suicide |
| *MS 3* | 66 | F | Active | Chronic progressive | Euthanasia |
| *MS 4* | 50 | F | Active; Chronic active | Chronic progressive | Euthanasia |
| *MS 5* | 77 | F | Chronic active | Chronic progressive | Euthanasia |
| *MS 6* | 86 | M | Chronic active | Chronic progressive | Heart failure |
| *NDC 1* | 72 | F | NDC | NA | Euthanasia |
| *NDC 2* | 72 | M | NDC | NA | Heart failure |

NDC, non-demented control; M, male; F, female; NA, not applicable.

## Mice

OSMRβ KO mice (B6.129S-Osmr <tm1Mtan>) were provided by the RIKEN BRC through the National Bio-Resource Project of MEXT, Japan, and were generated as previously described [48, 61]. All mice had a C57BL/6JOlaHsd background and WT mice were back-crossed with the genetically modified mice to obtain a genetically identical background. Mice were housed in an accredited conventional animal facility under a 12h light/dark cycle and had free access to food and water. All animal procedures were in accordance with the EU directive 2010/63/EU and all mouse experiments were approved by the Hasselt University Ethics Committee for Animal Experiments.

## EAE induction

Female WT and OSMRβ KO mice between 10 to 12 weeks of age were subcutaneously injected with myelin oligodendrocyte glycoprotein $(MOG)_{35-55}$ emulsified in complete freund's adjuvant (CFA) containing Mycobacterium tuberculosis, according to manufacturer's instructions (Hooke Laboratories, Lawrence, MA, USA). Immediately after immunization, mice were injected intraperitoneally (i.p.) with 40ng/100µl pertussis toxin (PTX). All mice were weighed daily and neurological deficits were evaluated using a standard 5-point scale (0: no symptoms; 1: limp tail; 2: weakness of hind legs; 3: complete paralysis of hind legs; 4: complete hind and partial front leg paralysis; 5: death). Analysis of the clinical EAE scores was performed using pooled data from three independent experiments (WT, n=30; OSMRβ KO, n=33). For post-mortem analysis of the CNS, transversal halves of the spinal cords were snap-frozen from naive mice, and at EAE onset (13 days post induction (dpi)), EAE peak (19 dpi) and the chronic phase of disease (50 dpi for histological analysis and 33 dpi for RNA analysis). To evaluate the immune cell profile by flow cytometry, immune cells were isolated from the CNS (pooled brain and spinal cord), draining lymph nodes and spleen at EAE onset (13 dpi), peak (19 dpi) and chronic phase (50 dpi) as described before [8]. Only mice with an EAE score > 0 were included in the analysis of the percentage of CNS-infiltrating cells at peak and chronic phase. A single cell suspension from lymph nodes and spleen was derived by mechanical transfer through a 70µm cell strainer (Greiner Bio-One, Vilvoorde, Belgium). For the CNS, both enzymatic digestion, using collagenase D (Roche Diagnostics GmbH, Mannheim, Germany) and DNase I (Roche Diagnostics GmbH), and mechanical dissociation was performed, followed by a Percoll gradient (GE Healthcare, Diegem, Belgium).

To assess T cell priming, spleens were isolated from MOG-immunized mice at 10 dpi and mechanically dissociated. Cells were cultured in RPMI-1640 medium (Lonza, Basel, Switzerland) containing 10% fetal calf serum (FCS, Biowest, Nuaillé, France), 1% non-essential amino acids (Gibco), 1% sodium pyruvate (Gibco), and 0.5% penicillin/streptomycin antibiotic-antimycotic solution (Life Technologies, Merelbeke, Belgium). Cells were labelled with CFSE to quantify T cell proliferation and stimulated with $MOG_{35-55}$, ConA or left untreated. After 4 days, CFSE incorporation was acquired on BD LSRFortessa™ (BD Biosciences) and analysed using BD FACSDiva™ Software (BD Bioscience). Results are expressed as stimulation index, calculated by dividing the percentage proliferating lymphocytes exposed to MOG antigen or ConA by the percentage of unstimulated cells. A minimum of 3 mice was assessed per condition.

## Cell culture

*Human peripheral blood mononuclear cells and functional assays*

Peripheral blood mononuclear cells (PBMCs) were isolated from whole blood using density gradient centrifugation (Ficoll-Paque™ PLUS, GE Healthcare). PBMCs were cultured in RPMI-1640 medium (Lonza) supplemented with 10% FCS, (Gibco™, Thermo Fisher Scientific, Waltham, MA, USA), 1% nonessential amino acids, 1% sodium pyruvate and 0.5% penicillin/streptomycin antibiotic-antimycotic solution (all Life Technologies). Cells were analysed *ex vivo* or after activation with 2 µg/ml anti-CD3 antibody (clone 2G3, BIOMED) or 2 µg/ml CpG2006 (ODN2006, InvivoGen, Toulouse, France) at 37°C/5% $CO_2$. OSMR expression was determined using flow cytometry.

For $CD4^+$ T cell, $CD8^+$ T cell and B cell proliferation assays, positive selection of $CD8^+$ T cells from PBMCs using magnetic beads was performed according to the manufacturer's protocol (MojoSort CD8 nanobeads, Biolegend, San Diego CA, USA). The untouched $CD8^-$ portion of PBMCs was used for positive selection of $CD4^+$ T cells using magnetic beads, according to the manufacturer's protocol (MACS CD4 Microbeads, Miltenyi Biotec, Bergisch Gladbach, Germany). B cells were negatively selected by magnetic separation (Mojosort™ Human B cell ($CD43^-$) Isolation Kit, BioLegend) from PBMCs. Isolated $CD4^+$ and $CD8^+$ T cells were labelled with 5 µM CellTrace™ Violet (Thermo Fisher Scientific), and isolated B cells were labelled with 1µM CFSE (CFSE Cell Division Tracker Kit, BioLegend) according to the manufacturer's protocol. Cells were seeded at a density of 2 x $10^5$ cells/well in the above mentioned culture medium in a 96-well U-bottom plate. T cells were activated with Treg suppression inspector beads (bead:cell ratio of 1:1; αCD3/CD28/CD2-coated beads, Miltenyi Biotec) and B cells were stimulated with 1 µg/ml CpG2006 (ODN2006, InvivoGen). Cells were either treated with 25 ng/ml rhOSM plus 20 µg/ml human LIFRα antibody, or with goat IgG isotype control (all R&D Systems). Cells that were treated with OSM received an additional treatment boost with 25 ng/ml OSM at day three. At day six, supernatant was collected and stored at −20 °C, LEGENDplex™ multiplex assay (Biolegend) was performed on CD8 T cell conditioned medium to determine concentrations of IL4, IL17, IFNγ, Granzyme A, Granzyme B and perforin according to manufacturer's instructions. T cell proliferation and B cell viability, proliferation and activation were analysed using flow cytometry.

For *in vitro* Th cell differentiation, $CD4^+$ memory T cells were separated from total PBMCs of healthy controls using memory $CD4^+$ T cell isolation kit (130-091-893, Miltenyi Biotec, Leiden, The Netherlands). Cells were cultured in 24-well plates at a density of 5 x $10^5$ cells and activated with 2.5 µg/ml plate-bound human anti-CD3 (clone OKT3, Invitrogen™, Thermo Fisher Scientific) and 2 µg/ml soluble anti-CD28 (clone CD28.2, BD Biosciences). Th1 cell differentiation was induced by adding 10 ng/ml recombinant human (rh)IL-12 and 5 µg/ml anti-IL-4 antibody, while Th17 cell differentiation was induced by 25 ng/ml rhIL-23, 5 µg/ml anti-IL-4 antibody and 5 µg/ml anti-IFNγ antibody (all R&D Systems). Cells were expanded for 5 days at 37°C/5% $CO_2$. Cytokine production was analysed using flow cytometry as measure for Th cell differentiation.

*Human brain-derived endothelial cells*

The human cerebral microvascular endothelial cell line hCMEC/D3 was provided by Tebu-bio (Le Perray-en-Yvelines, France) and cultured using the EGM™-2 MV Microvascular Endothelial Cell Growth Medium-2 BulletKit™ (CC-3202, Lonza), in 75 µg/ml collagen type I (Merck)-coated plates or inserts at 37°C/5% $CO_2$. When 80% confluent, medium was changed to EBM™-2 Basal Medium (CC-3156, Lonza) supplemented with 5 ng/ml human fibroblastic growth factor (FGF), 1.4 µM hydrocortisone, 10 mg/ml gentamicin, 1 mg/ml amphotericin (A2942, all Merck) and 2.5% FCS (Gibco™, Thermo Fisher Scientific). Cells were treated for 24h or 48h with 25 ng/ml rhOSM (R&D systems), or left untreated, in resting or activating conditions, in serum-reduced (0.25% FCS) EBM-2 medium without hydrocortisone. Inflammation was induced by pro-inflammatory cytokines, 10 ng/ml rhTNFα and 10 ng/ml rhIFNγ (Peprotech, London, UK), at the time of OSM treatment. For flow cytometric analysis, cells were detached after 48h treatment using trypsin (T4549, Merck) or by scraping.

*Primary human brain microvascular endothelial cells*

Primary human brain microvascular endothelial cells (HBMECs) were isolated from non-epileptic material according to a published protocol [8, 13, 43]. Informed consent and ethic approval were obtained before surgery (Centre Hospitalier de l'Université de Montréal research ethic committee approval 20.332-YP). In brief, the meninges were removed and brain tissue was minced, resuspended in PBS and washed multiple times to remove blood. After homogenization, CNS material was filtered through one 350µm and two 112µm pore size meshes (BSH Thompson, Montreal, Quebec, Canada). Cells were cultured on 0.5% gelatin-coated six-well plates, in EC culture media composed of M199 cell culture media (Thermofisher Scientific) supplemented with 10% FBS, 5% human normal serum (Gemini), 0,2% insulin-transferrin-sodium selenite 100X (Sigma-Aldrich), and 0,14% EC growth supplement (BD Biosciences) at 37°C/5% $CO_2$. When confluent, cells were treated for 48h with 25 ng/ml rhOSM (R&D Systems), in presence or absence of rhTNFα (100 U/mL) and rhIFNɣ (100 U/mL, both Thermo Fisher Scientific). After stimulation, conditioned medium was collected and cells were washed with PBS and gently detached using 1x Trypsin-PBS-EDTA (Thermo Fisher Scientific), after which cells were immediately processed for flow cytometry experiments.

*Human choroid plexus epithelial cells*

Choroid plexus papilloma cells (HIBCPP) were cultured as described [27, 52, 62]. In short, HIBCPP cells were cultured in 24 well plates (Greiner bio-one) in DMEM/HAM's F12 1:1 (Gibco) supplemented with 4 mM L-Glutamine (Gibco), 5 µg/ml insulin (I9278, Sigma), penicillin (100 U/ml) and streptomycin (100 µg/ml) (Lonza), 15% (v/v) heat inactivated FCS (Life Technologies). Confluent monolayers were subsequently treated for 48h with 25 ng/ml rhOSM (R&D Systems), in presence or absence of rhTNFα and rhIFNɣ (10 ng/ml, Preprotech). After stimulation, conditioned medium was stored at -20°C for further processing.

*Human astrocytes*

Human astrocytes (HA, ScienCell, Carlsbad, CA, USA) were cultured according to the manufacturer's protocol. In short, HA cells were cultured in poly-L-lysine (PLL, 2µg/cm²)-coated well plates in astrocyte medium supplemented with 2% FBS, 1% astrocyte growth supplement and 1% penicillin/streptomycin (all Sciencell). Cells were treated for 48h with 25 ng/ml rhOSM (R&D Systems), in presence or absence of rhTNFα and rhIFNɣ (10 ng/ml, Preprotech). After treatment, medium was stored at -20°C for further processing.

*Primary mouse brain microvascular endothelial cells*

Primary mouse brain microvascular endothelial cells (MBMECs) were isolated from 4- to 6-week-old WT and OSMRβ KO mice. Brains were dissected, and meninges and choroid plexuses were removed. Remaining parenchymal brain tissue was minced, homogenized, and digested with DMEM containing 1.05 mg/ml collagenase type II (Gibco™, Thermo Fisher Scientitic) and 58.5 U/ml DNase I for 75 min at 37°C on a shaker (150 rpm). Myelin was removed by a 20 min centrifugation step at 1000g in 20% bovine serum albumin (BSA, Merck) in DMEM. The remaining pellet was further digested with 1 mg/ml collagenase/dispase (Roche Diagnostics GmbH) and 39 U/ml DNase I in DMEM for 1h at 37°C on a shaker (150 rpm). Brain microvessels were obtained using a 33% continuous Percoll gradient, centrifuged at 1000g for 10 min. The resulting primary ECs were plated in 10 µg/ml collagen type IV (Merck)-coated well plates or inserts. MBMECs were cultured in DMEM supplemented with 20% FCS (Biowest), 1 ng/ml FGF, 100 µg/ml heparin, 1.4 µM hydrocortisone (all Merck) and 0.5% penicillin/streptomycin antibiotic-antimycotic solution. Cells were cultured at 37°C/5% $CO_2$. Until 48h after plating, cells were grown in medium containing 10 µg/ml puromycin (Sigma-Aldrich) to obtain pure EC cultures. In the next 24h, puromycin concentration was decreased to 4 µg/ml. Thereafter, cells were cultured in medium without additional puromycin. When confluent, cells were treated with 25 ng/ml rmOSM (R&D Systems), in resting and activating conditions. Inflammation was induced by pro-inflammatory cytokines, 10 ng/ml rmTNFα and 10 ng/ml rmIFNγ (Peprotech). For flow cytometric analysis, cells were detached using trypsinization.

*Primary mouse astrocytes*

Primary mouse astrocytes were isolated as previously described [24]. In short, brains of P0-P2 WT C57BL/6J pups were dissected and meninges were removed. A mixed glial cell cultures was obtained and cultured at 37°C/8.5% $CO_2$. After 14 days, non-adherent cells, i.e. oligodendrocytes and microglia, were removed by vigorously shaking to obtain primary astrocytes. One day after plating, the cells were treated for 48h with 25 ng/ml rmOSM (R&D Systems), in presence or absence of rmTNFα and rmIFNɣ (10 ng/ml, Preprotech) at 37°C/5% $CO_2$. Conditioned medium was stored at -20°C for further processing.

## Flow cytometry

To asses T cell proliferation, T cells were stained with fixable viability dye eFluor780 (eBioscience™, Thermo Fisher Scientific), and CellTrace Violet dilution was determined using flow cytometry. Unlabelled stimulated cells that received no treatment, as well as labelled unstimulated cells were used as controls to set proliferation gates. B cell viability, proliferation and activation were assessed using Fixable Viability Dye eFluor780 and the following anti-human monoclonal antibodies: CD19 BV650, CD24 BV605, CD38 BV711, CD80 PE-Dazzle594, CD86 BV785, Gp130 PE (all from BioLegend), CD25 PE-Cy7 (Invitrogen, Thermo Fisher Scientific) and OSMR APC (eBioscience™). For intracellular cytokine staining, cells were stimulated for 4h with phorbol 12-myristate 13-acetate (PMA, Merck), ionomycin (Merck) and Golgiplug or Golgistop (BD Biosciences, Erembodegem, Belgium) to boost cytokine production, and permeabilized using BD Cytofix/Cytoperm™ Fixation/Permeablization Kit (BD Biosciences). Zombie NIR (BioLegend), fixable viability dye eFluor™ 506 (eBioscience™) or LIVE/DEAD fixable Aqua dead cell stain kit (Thermo Fisher Scientific) were used as live/dead staining. For phenotyping mouse cells, the following antibodies were used: anti-mouse CD45 Alexa Fluor® 700, CD3 FITC, CD4 Pacific Blue™, CD8 Brilliant Violet™ 510, CD19 Brilliant Violet 650™, CD11b PERCP/Cy5.5, Ly6C Brilliant Violet™ 785, IL-4 PE, IL-17 PE/Dazzle™ 594, IFNγ PE-Cy7 and Foxp3 Alexa Fluor® 647 (all Biolegend), ICAM-1 Alexa Fluor® 647 (Molecular Probes, Life technologies) and VCAM-1-FITC (eBioscience™, Thermo Fisher Scientific). For phenotyping human cells, the following antibodies were used: anti-gp130-FITC (Abcam, Cambridge, UK) and anti-OSMRβ-PE antibodies (eBioscience™, Thermo Fisher Scientific) combined with PerCP-labeled antibodies specific for the immune cells subsets, CD3, CD4, CD8, CD14 and CD19 (all BD Biosciences). Cytokine staining was performed using following antibodies: anti-human IFNg PERCP Cy5.5, IL4 PE-Cy7 (Biolegend) and IL-17 PE (eBioscience™). HBMECs and hCMEC/D3 cells were analysed using following antibodies: anti-human ICAM-1 (CD54) PE/Dazzle™ 594, VCAM-1 (CD106) APC, VE-cadherin FITC (all Biolegend), ICAM-1 PE and VCAM-1 FITC (BD Biosciences). Our gating strategy excluded doublets (using classical gating strategy) and dead cells, and defined positive gates using fluorescence minus one (FMO) controls. Samples were acquired on BD LSRFortessa™, FACSCalibur or BD™ LSRII cytometer (BD Biosciences) and analysed using FlowJo 10.8.0, CellQuest Software or FACSDiva™ Software (BD Bioscience).

## Immunohistochemistry

Diaminobenzidine (DAB) immunohistochemistry was performed on 10 µm cryosections from post-mortem human brain material (Table 2). Classification of the type of MS lesion was done based on PLP and HLA-DR staining by the Netherlands Brain Bank and confirmed at our institute based on PLP and CD68 staining. Sections were fixed in acetone after which they were blocked using Dako® protein block (Agilent, Santa Clara, CA, USA). Subsequently, sections were incubated with the primary antibody overnight at 4°C: mouse-anti-PLP (1:100, Bio-Rad, Hercules, CA, USA), mouse-anti-CD68 (1:100, Dako, Agilent), rabbit-anti-OSM (1:50, Thermo Fisher Scientific), rabbit-anti-CCL20 (1:500, Abcam). Next, sections were incubated with EnVision+ Dual Link reagent (Dako, Agilent) for 30 min, followed by visualization with peroxidase substrate DAB. In addition, sections were counterstained with haematoxylin followed by extensive washing. Sections were dehydrated with ethanol and xylene and mounted with DPX. Microscopic analysis was performed using Leica DM2000 LED (Leica Microsystems, Heidelberg, Germany).

For immunofluorescent stainings, post-mortem human brain sections were fixed in acetone and blocked with Dako® protein block in PBS/0.05% Tween20. Next, sections were incubated with rabbit-anti-OSM (1:50) combined with mouse-anti-GFAP (1:400, Merck) or mouse-anti-CD68, or rabbit-anti-CCL20 (1:500) combined with mouse-anti-CD31 (1:100, Dako, Agilent) as primary antibodies at 4°C overnight. Immunoreactivity was visualized using goat anti-mouse Alexa Fluor 488 and donkey-anti-rabbit Alexa Fluor 555 (Invitrogen™, Thermo Fisher Scientific), after 1h incubation at room temperature. Nuclear staining was performed with 4',6-diamidino-2-phenylindole (DAPI). Finally, sections were incubated with 0.3% Sudan Black (Merck) in 70% ethanol to limit autofluorescence and mounted with Fluoromount-G™ Mounting Medium (Invitrogen™, Thermo Fisher Scientific). Microscopic analysis was performed using Leica DM2000 LED and Leica Application Suite X (LAS X) software (Leica Microsystems).

Murine spinal cord tissue was cryosectioned into 10 µm sections using the Leica CM3050S cryostat (Leica Microsystems). Sections were fixed in acetone, blocked with Dako® protein block and incubated with rabbit anti-laminin (1:2000, Abcam) and donkey anti-IgG Alexa 488 (1:800, Thermo Fisher Scientific), or rabbit-anti-CCL20 (1:500). Binding of the primary antibody against laminin or CCL20 was visualized using goat-anti-rabbit Alexa 555-conjugated secondary antibody (Life technologies) and nuclear staining was performed with DAPI. Autofluorescence was counteracted using Sudan Black (0.3% in 70% EtOH). Microscopic analysis was performed using Leica DM2000 LED and Leica Application Suite X (LAS X) software. Six pictures were taken at 3 different levels in the spinal cord, resulting in 18 pictures per mouse. The mean IgG or CCL20 intensity was quantified using auto threshold in ImageJ (FIJI).

### Quantitative PCR

RNA was isolated from snap-frozen CNS tissue of WT and OSMRβ KO mice using the RNeasy Lipid Tissue Mini Kit (Qiagen, Venlo, The Netherlands) according to manufacturer's instructions. MBMECs and hCMEC/D3 cells were collected in RLT buffer containing 1% β-mercaptoethanol, after 24h treatment. RNA isolation was performed according to the RNeasy® Mini Kit (Qiagen) manufacturer's protocol. Concentrations were measured using NanoDrop™ 2000/2000c Spectrophotometer (Thermo Fisher Scientific). Conversion of RNA to cDNA was performed using qScript™ cDNA SuperMix (Quanta Biosciences, Beverly, MA, USA). Quantitative PCR was performed utilizing a StepOnePlus Real-Time PCR detection system (Life technologies) and universal cycle conditions (20s at 95°C, 40 cycles of 3s at 95°C and 30s at 60°C). The PCR reaction consisted of SYBR™ Green PCR Master Mix (Applied Biosystems, Thermo Fisher Scientific), 10µM forward and reverse primer (Integrated DNA Technologies, Leuven, Belgium) (Table 3), RNase free water and 12.5ng template cDNA. Expression was normalized using the two most stable housekeeping genes, computed using geNorm software version 3.5. ΔΔCt values were converted to fold change as compared to experimental control.

**Table 3** Primer sequences

| | Forward primer (5' – 3') | Reverse primer (5' – 3') |
|---|---|---|
| *mOSMRβ* | TCACAACTCCAGATGCACGC | ACTTCTCCTTCACCCACTGAC |
| *mICAM-1* | GCCTTGGTAGAGGTGACTGAG | GACCGGAGCTGAAAAGTTGTA |
| *mVCAM-1* | TGCCGAGCTAAATTACACATT | CCTTGTGGAGGGATGTACAGA |
| *mHPRT* | CTCATGGACTGATTATGGACAGGAC | GCAGGTCAGCAAAGAACTTATAGCC |
| *mTBP* | ATGGTGTGCACAGGAGCCAAG | TCATAGCTACTGAACTGCTG |
| *mHMBS* | GATGGGCAACTGTACCTGACTG | CTGGGCTCCTCTTGGAATG |
| *mYWHAZ* | GCAACGATGTACTGTCTCTTTTGG | GTCCACAATTCCTTTCTTGTCATC |
| *hCCL20* | CCCAAAGAACTGGGTACTGAAC | GCAGTCAAAGTTGCTTGCTG |
| *hOSMRβ* | CCAGAGTGAAGTCCTGGCTGA | TGTAAGTGCAAACTCTGAGCG |
| *hICAM-1* | AGCTTCGTGTCCTGTATGGC | ACAGTCACTGATTCCCCGAT |
| *hICAM-2* | CCAGAGCTACCCTTCTTGGA | CCTCGACACTGCCAAAATCC |
| *hICAM-3* | TTCTTCTGCAGTGCCACTCT | TGTGGCTCGGTCAATTTTGG |
| *hTBP* | TATAATCCCAAGCGGTTTGC | GCTGGAAAACCCAACTTCTG |
| *hYWHAZ* | CTTGACATTGTGGACATCGG | TATTTGTGGGACAGCATGGA |

OSMRβ, oncostatin M receptor beta; ICAM-1, intercellular cell adhesion molecule 1; VCAM-1, vascular cell adhesion molecule 1; HPRT, hypoxanthine phosphoribosyltransferase; TBP, TATA binding protein; HMBS, Hydroxymethylbilane synthase; YWHAZ, Tyrosine 3-Monooxygenase/Tryptophan 5-Monooxygenase Activation Protein Zeta; CCL20, C-C motif ligand 20

### Human chemokine array and Enzyme linked immunosorbent assay (ELISA)

Conditioned medium of hCMEC/D3 cells, MBMECs, primary mouse and human astrocytes, and HIBCPP cells was collected after 48h stimulation. For hCMEC/D3 cells, 31 human chemokines were analysed using the Proteome Profiler Human Chemokine Array Kit (R&D systems) according to the manufacturer's instructions. Spot density was imaged using Amersham™ imager 680 and quantified using ImageQuant TL (GE Healthcare). The spot volume of each chemokine relative to the internal positive control was normalized to control medium as semi-quantification method. CCL20 was selected from the human chemokine array and chemokine production was validated by Human MIP-3α (CCL20) Pre-Coated ELISA Kit (Biogems, Peprotech) and Mouse MIP-3α (CCL20) ELISA Kit (Invitrogen™, Thermo Fisher Scientific) following the manufacturer's instructions in conditioned medium of hCMEC/D3 cells, MBMECs, primary mouse and human astrocytes, and HIBCPP cells. Absorbance was measured at 450 nm using a Tecan plate reader (Tecan, Männedorf, Switzerland).

### Flow cytometric FRET assay

To quantify integrin αL activation based on conformational changes, fluorescence resonance energy transfer (FRET) was measured using flow cytometry [10, 54, 64]. *In vitro* differentiated Th17 cells (on average 18.2 ± 8.6% IL-17 producing cells) were incubated with basal medium (with or without 1 µg/ml rhCCL20) or hCMEC/D3 cell conditioned medium (48h stimulated with rhOSM, TNFα and IFNγ) for 15 min at 37°C, at $10^7$ cells/ml, to trigger chemokine-induced integrin activation. Afterwards, cells and buffers were kept on ice during the whole procedure. Fixable viability dye eFluor™ 506 (eBioscience™) was used as live/dead staining on all samples. Anti-human CD11a FITC antibody (clone HI111, Biolegend) was incubated for 30 min and used as donor molecule (D)

since it binds the top region of the I domain of integrin $\alpha_L$. Octadecyl Rhodamine B Chloride (R18, Invitrogen™, Thermo Fisher Scientific) was incubated for 20 min at 1 µg/ml and used as acceptor molecule (A) since it stains the lipid cell membrane. Cells were washed and resuspended in staining buffer (PBS/1% FCS/0.1% Na-azide). Samples were acquired on BD FACSAria™ Fusion Flow Cytometer (BD Biosciences) with 405, 488 and 561 nm lasers and analysed using FlowJo 10.8.0 software (BD Biosciences). Transfer of energy from D to A causes a decrease in the fluorescence intensity in the FITC channel, depending on the proximity of the D to A in the membrane (Fig. 5C). Therefore, we determined $\Delta MFI = F_D - F_{DA}$ as an estimate of FRET occurrence, where $F_D$ is the donor fluorescence in the absence of acceptor and $F_{DA}$ is the donor fluorescence in the presence of acceptor. A closed integrin conformation (inactive) promotes energy transfer between D and A and thereby increases ΔMFI.

### Th17 cell adhesion assays

A modified Boyden chamber assay was performed to quantify T cell adhesion. hCMEC/D3 were seeded in collagen-coated Thincerts (24 well, translucent, 3 µm, Greiner bio-one) at a density of $25x10^3$ cells/cm². After 5 days, cells were treated with TNF-α (10 ng/ml) and IFN-γ (10 ng/ml, all Peprotech) with or without 25 ng/ml rhOSM (R&D systems) for 24h. Before starting migration, hCMEC/D3 were pre-incubated with either 10 µg/ml isotype control (mouse IgG1, R&D systems) or 10 µg/ml human ICAM-1/CD54 Antibody (R&D systems) for 2h at 37°C. Differentiated Th17 cells (on average 19.8 ± 5.4% IL-17 producing cells) were loaded ($5x10^5$) onto replenished inserts (in duplo) and were allowed to migrate for 24h. After migration, inserts were washed and fixed with 4% PFA for further nuclear staining with DAPI. The membrane was separated from the insert and mounted on a glass slide with Fluoromount-G™ Mounting Medium (Invitrogen™, Thermo Fisher Scientific). Microscopic analysis was performed using Leica DM2000 LED and Leica Application Suite X (LAS X) software. Six pictures were taken per insert (in duplo) resulting in 12 pictures/condition per experiment. The number of T cell nuclei was quantified based on cell diameter using ImageJ.

Secondly, a flow system adhesion assay was performed using the Ibidi pump system (ibidi GmbH, Gräfelfing, Germany). hCMEC/D3 cells were cultured to confluency on a 0.4 mm µ-slide™ (ibidi GmbH). Cells were pre-treated for 24h with 10 ng/ml rhTNFα, IFNγ and 25 ng/ml OSM and then incubated with human ICAM-1/CD54 antibody (10 µg/ml, BBA3, R&D systems) or mouse IgG1 isotype control (10 µg/ml, MAB002, R&D systems) 2h prior to the addition of Th17 cells. *In vitro* differentiated Th17 cells (on average 20.8 ± 3% IL-17 producing cells) were labelled with Tag-it Violet™ dyes (Biolegend) or CellTrace™ CFSE (Invitrogen™, Thermo Fisher Scientific) according to manufacturer's instructions, of which the latter was pre-incubated with 1 µg/ml rhCCL20 for 15 min at 37°C to promote integrin activation, prior to adding them to hCMEC/D3 cells. The µ-slide™ was connected to the flow system using the grey perfusion set (100cm tubing length, 0.8mm diameter, ibidi GmbH). Labelled Th17 cells were added to the flow system in a 1:1 ratio, at $10^6$ cells/ml. An increasing shear stress starting from 0.1 up to 0.56 dyn/cm² (physiological) was applied for 25 min [32]. Live time-lapse videos were generated using Zeiss Elyra PS.1 (10x objectives, 1.6x lens, 300 frames, every 5s). Cell adhesion was evaluated using the TrackMate plugin in ImageJ [63].

### Transendothelial electrical resistance

To quantify BBB integrity, MBMECs were grown to confluency on collagen-coated transwell inserts in a 24-well plate (3 µm pore size, transparent Thincerts™, Greiner bio-one). TEER (in Ω) was measured across a monolayer of ECs using the EVOM² resistance meter (World Precision Instruments, Florida, USA). Collagen-coated transwell inserts containing medium without cells were used as a blank. The background resistance was subtracted from the resistance values of cell-containing inserts. When reaching a plateau phase, MBMECs were stimulated for 48h. TEER values were measured every 24h, from the day after cell seeding until 48h after treatment. Data are depicted as Ω x cm², based on the insert surface area (0.336 cm²).

hCMEC/D3 cells were grown to confluency on collagen-coated 16-well RTCA E-Plates (Agilent, Santa Clara, CA, USA), containing interdigitated gold microelectrodes, covering approximately 70-80% of the surface of each well. TEER (in Ω) was measured over a frequency range from 1Hz to 1000 kHz at 5 frequencies per decade. A PalmSens 4 impedance analyser, controlled by PSTrace software (PalmSens BV, Houten, The Netherlands), automatically conducted measurements every 20 min. Using the MUX8-R2 multiplexer (PalmSens BV), changes in the TEER of up to 8 different electrode pairs could be followed simultaneously. Data analysis was performed using a custom-made in-house Python script. When maximum barrier resistance was reached, cells were stimulated for 48h. As at the mid-frequency range, the cell-related TEER parameter contributes predominantly to the total impedance [6], values were analysed at a frequency of 6309.57 Hz, reflecting these intercellular junctions, and data are depicted as Ω x cm², based on the well's surface area (0.196 cm²).

### Protein isolation and western blot

To examine claudin-5 protein expression, hCMEC/D3 cells and MBMECs were collected after 48h treatment and lysed with RIPA lysis buffer containing 150 mM sodium chloride, 1% Triton X-100, 0.5% sodium deoxycholate, 0.1% SDS, 50 mM Tris and protease inhibitors (Roche Diagnostics GmbH) for protein isolation. Protein yield was quantified using the Pierce™ BCA Protein Assay kit (Thermo Fisher Scientific) according to manufacturer's guidelines. The maximal amount of denatured protein was loaded, separated on a 12% SDS polyacrylamide gel and transferred to a polyvinylidene (PVDF) membrane (Merck). After blocking with 5% skimmed milk in Tris-buffered saline-0.1% Tween20 (TBS-T), the membrane was incubated with rabbit anti-Claudin-5 (1:500 in TBS-T containing 0.01% sodium azide, Invitrogen™, Thermo Fisher Scientific) overnight at 4°C. Afterwards, the membrane was washed with TBS-T, followed by a 1h incubation with HRP-labelled goat anti-rabbit (Dako, Agilent). Bands were developed with ECL plus substrate (Thermo Fisher Scientific) and analysed with Amersham™ imager 680 (GE Healthcare). A decrease in claudin-5 expression upon TNFα/IFNγ stimulation served as positive control. β-actin was used as reference loading control using mouse anti-β-actin as primary antibody (1:10000; Santa Cruz Biotechnology, Heidelberg, Germany) and HRP-labeled rabbit anti-mouse (Dako, Agilent) as secondary antibody. Band density was quantified using ImageQuant TL (GE Healthcare).

## Statistical analysis

Statistical analysis was performed using GraphPad Prism 9.1 (GraphPad software Inc., CA, USA). Differences between group means were determined using Mann-Whitney test, one-way ANOVA with Dunnett's or Šidák's multiple comparison test, and two-way ANOVA with Šidák's multiple comparison test. For *in vitro* BBB-EC assays, pre-selected comparisons were made, including Control vs. OSM; Control vs. TNFα/IFNγ; Control vs. OSM + TNFα/IFNγ; TNFα/IFNγ vs. OSM + TNFα/IFNγ. Data are depicted as mean ± standard error of the mean (SEM) *=$p<0.05$, **=$p<0.01$, ***=$p<0.001$ and ****=$p<0.0001$. For all experiments biological replicates were conducted.

## Results

### OSMR is highly expressed on circulating lymphocytes in untreated MS patients

Since it is established that OSM levels are increased in the blood and CNS of MS patients [16, 25, 53], we sought to determine whether lymphocytes are responsive to OSM based on their receptor expression and whether their expression is altered during MS pathogenesis. To this end, we determined OSMR expression (composed of the OSMRβ and gp130 subunits) on T and B cells isolated from the blood of HC, untreated and treated MS patients using flow cytometry. In untreated MS patients, increased numbers of $CD4^+$ T helper cells (25.40% vs 1.83%) expressed OSMRβ-gp130 as compared to HC (Fig. 1a). A similar increase was detected in $CD8^+$ cytotoxic T cells (20.93% vs 0.71%) and $CD19^+$ B cells (18.16% vs 4.27%) (Fig. 1c, e). Interestingly, circulating lymphocytes of treated MS patients show a significantly lower OSMRβ-gp130 receptor expression compared to untreated MS patients (Fig. 1a, c, e). To examine whether activation of lymphocytes augments OSMR expression, HC-derived PBMCs were activated with anti-CD3 antibody or CpG to activate T or B cells, respectively. Activation significantly increased OSMRβ-gp130 expression on $CD4^+$ T cells and $CD19^+$ B cells, while showing a trend for $CD8^+$ T cells (Fig. 1b, d, f). Next, we questioned whether OSM affects the functional properties of resting or activated $CD4^+$ T cells, $CD8^+$ T cells and $CD19^+$ B cells. In this regard, $CD4^+$ T helper cell proliferation and differentiation (Suppl. Fig. 1a-c), $CD8^+$ T cell proliferation, cytokine production and cytotoxic capacity (Suppl. Fig. 1d-f), and B cell proliferation, activation and plasmablast formation (Suppl. Fig. 1g-i) were examined. However, none of these functional properties were significantly affected by OSM in peripheral immune cells. Together, these data indicate that OSMR is upregulated on circulating lymphocytes in untreated MS patients, suggestively due to immune activation, whereas immunosuppressive therapies decrease OSMR expression.

### OSM is produced by activated macrophages/microglia and astrocytes in human MS lesions

To examine the contribution of OSM to MS brain pathology, we evaluated the expression of OSM in post-mortem MS brain tissue. Hereto, cellular localisation of OSM was examined in active and chronic active MS lesions (Fig. 2). OSM immunoreactivity was increased in active lesions (as characterized by demyelination and myeloid cell infiltration) compared to paired normal appearing white matter (NAWM) (Fig. 2a). In comparison, OSM immunoreactivity was more diffuse in chronic active lesions, with a less pronounced cellular localisation (Fig. 2a). In control brain tissue, limited OSM expression was observed (Fig. 2a). To identify the cell types that produce OSM within the brain, immunofluorescent double labelling studies were performed. We show co-localization of OSM with $CD68^+$ myeloid cells inside active lesions (Fig. 2b) and with $GFAP^+$ astrocytes at the lesion border and NAWM (Fig. 2c). These data indicate that OSM is highly expressed by the majority of activated macrophages/microglia in active MS lesions and by astrocytes in the surrounding white matter, suggesting an important role for OSM signalling during acute neuro-inflammation.

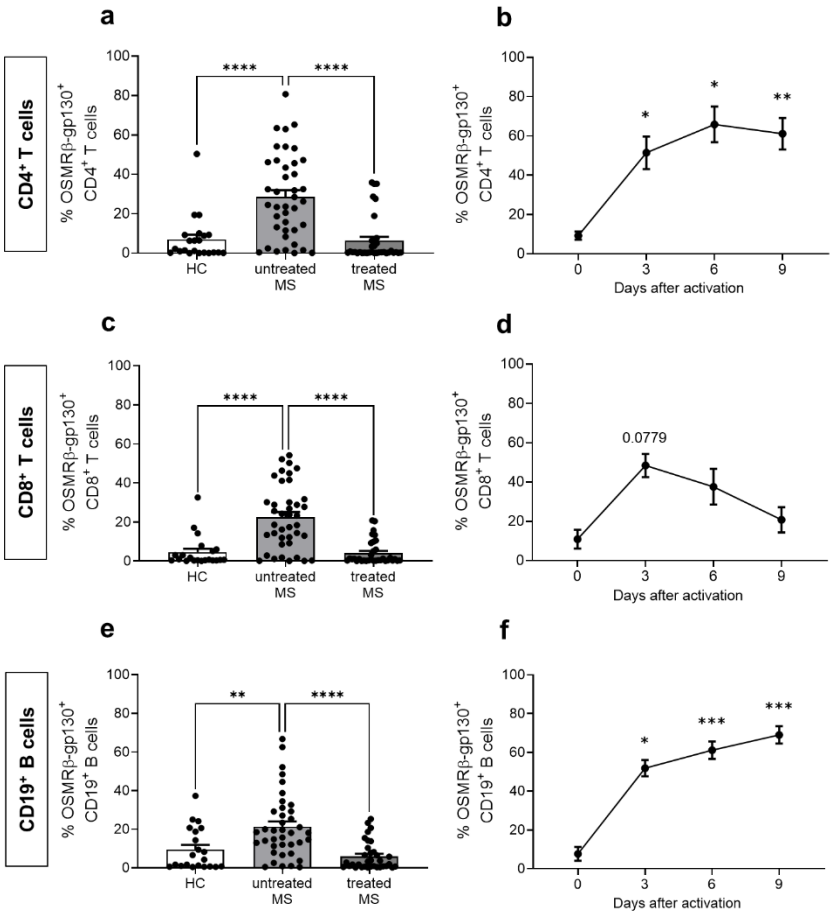


458 **Fig 1** OSMR expression is increased on circulating T and B cells of MS patients while immunosuppressive MS treatments
459 reduce its expression on circulating immune cells. **(a)** Percentage of CD4⁺ T helper cells, **(c)** CD8⁺ cytotoxic T cells and **(e)**
460 CD19⁺ B cells co-expressing OSMRβ and gp130 were measured in PBMCs of healthy controls (HC, n=22), untreated MS
461 patients (n=41) and treated MS patients (n=37; receiving IFN-β (n=19), glatiramer acetate (n=7) and natalizumab (n=11)) using
462 flow cytometry. Dots represent the percentage of positive cells in each donor. Expression of OSMRβ-gp130 after activation
463 of PBMCs of HC with anti-CD3 antibody (2 µg/ml) or CpG (2 µg/ml) on **(b)** CD4⁺ T helper cells (n=5), **(d)** CD8⁺ cytotoxic T cells
464 (n=4) and **(f)** CD19⁺ B cells (n=4). Data are depicted as mean ± SEM. Statistical analysis was performed using one-way ANOVA
465 and Tukey's or Dunnett's multiple comparisons test with *p≤0.05, **p≤0.01, ***p≤0.001, ***p≤0.0001.

466

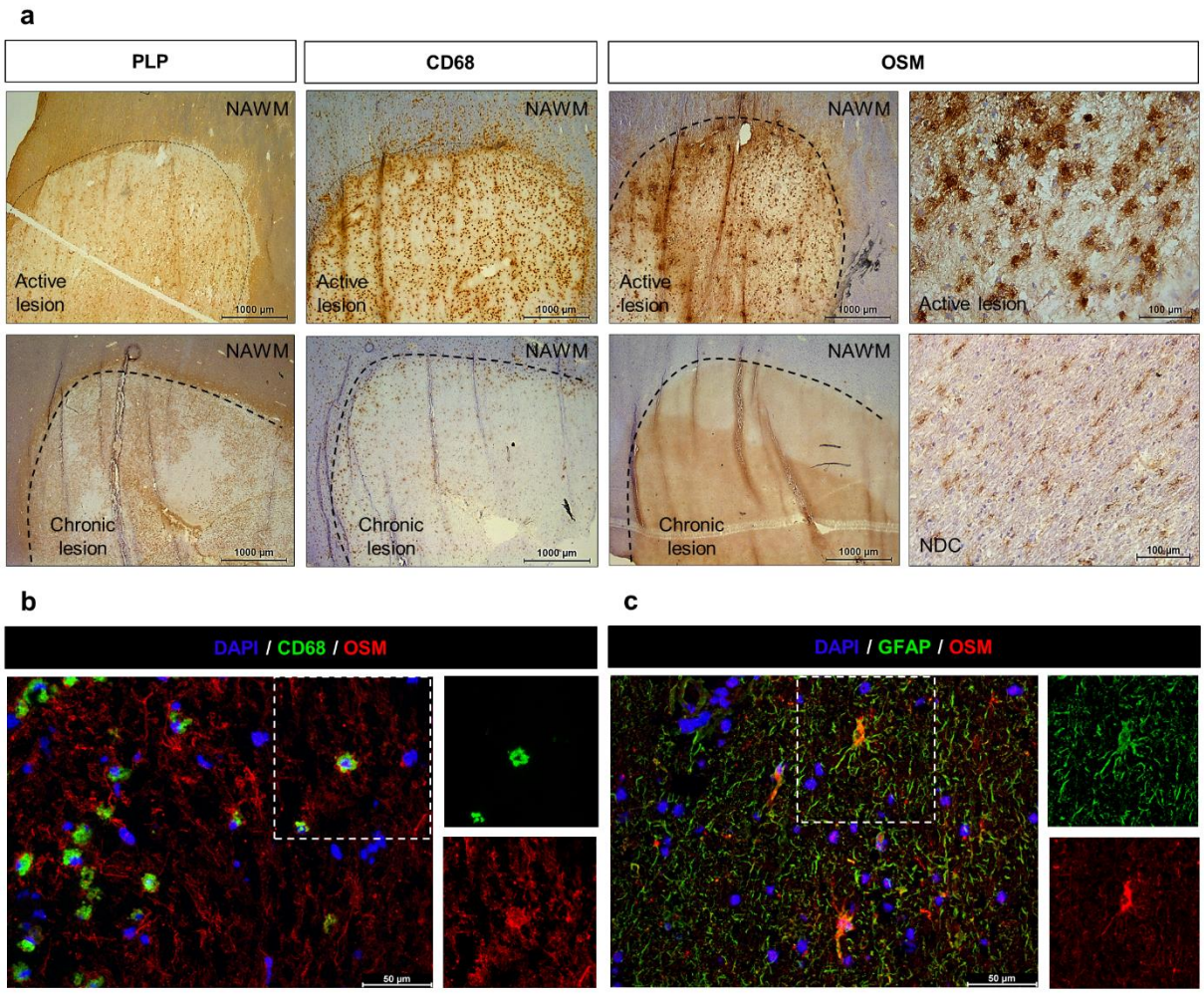


**Fig 2** OSM is expressed by activated myeloid cells and astrocytes in active MS brain lesions. **(a)** Immunostaining for PLP and CD68 identifies the demyelinated area with either dense myeloid cell infiltration (active MS lesion) or myeloid cells concentrated at the lesion border (chronic active MS lesion). The dotted line shows the approximate boundary between the demyelinating lesion and NAWM. OSM is highly expressed within the active lesion, while basal expression is detected in NAWM and NDC brain tissue. High magnification view of OSM expression in the active lesion centre suggests active myeloid cell morphology. Scale bars represent 1000 and 100 µm. **(b)** Immunofluorescence shows OSM (red) co-localization with $CD68^{+}$ activated myeloid cells (green) and **(c)** $GFAP^{+}$ astrocytes (green). Nuclear staining was performed with DAPI (blue). Separate channels are shown of the square surrounding single cells. Scale bars represent 50 µm. OSM, oncostatin M; PLP, proteolipid protein; NDC, non-demented control; NAWM, normal appearing white matter; GFAP, glial fibrillary acidic protein; DAPI, 4',6-diamidino-2-phenylindole.

## Milder EAE in OSMRβ-deficient mice is associated with decreased Th17 cell infiltration

Given the prominent expression of OSM and its receptor in the blood and brain of MS patients, we determined the contribution of OSM signaling to neuro-inflammation *in vivo* using the EAE model. First, an increase in OSMRβ mRNA levels was observed at peak and in the chronic phase of disease in the CNS of wild-type (WT) mice, implying an important role for this receptor during the disease process (Fig. 3a). Second, when EAE was induced in OSMRβ-deficient mice, we observed significantly milder EAE symptoms in OSMRβ KO mice (Fig. 3b, c, e). In addition, the incidence of EAE was lower in OSMRβ-deficient mice, i.e. 93.33% for WT mice and 75.76% for OSMRβ KO mice, resulting in a significantly different symptom-free survival rate (Fig. 3d). Interestingly, OSMRβ deficient mice showed a delayed and lower peak of disease, after which they did not recover in the way WT mice did (Fig. 3b). These results were confirmed by a significantly decreased area under the curve (AUC, Fig. 3f) and sum of EAE scores in OSMRβ-deficient mice (Suppl. Fig. 2a).

To find an explanation for the difference in clinical scores, the immune cell profile in draining lymph nodes, spleen and CNS was analyzed at onset, peak and chronic phase of disease using flow cytometry (gating strategy: see suppl. Fig. 2d). In peripheral lymphoid organs of OSMRβ-deficient mice, the percentages of Th1 ($IFN\gamma^+/IL17^-$) and Th17 ($IFN\gamma^-/IL17^+$) cells were unchanged, while the percentage of $Foxp3^+$ Tregs was increased compared to WT mice at peak of disease (Fig. 3g-l). Peripheral lymphocyte proliferation in response to *in vitro* MOG restimulation was unchanged in OSMRβ deficient mice (suppl. Fig. 2b). Together, these results suggest that the effect of OSM on the peripheral immune system is limited.

When analyzing infiltrating immune cells in the CNS compartment of WT and OSMRβ KO mice, we found a significantly reduced percentage of Th17 cells at onset and peak of disease in OSMRβ-deficient mice (Fig. 3n). This is also reflected in a decreased Th17 cell number of the total CNS-infiltrating cells at EAE peak, since the percentage Th17 cells show a positive correlation with Th17 cell counts, while Th1 cell numbers were unchanged (Suppl. Fig. 2e-g). Percentages of Th1 cells and $Foxp3^+$ Tregs (Fig. 3m, o) were unaffected in the CNS and no differences in the percentages of total infiltrating $CD4^+$ T cells (Suppl. Fig. 2c) or B cells (Suppl. Fig. 2k-m) were observed between genotypes. $CD8^+$ T cells were significantly increased in the chronic phase of disease in the CNS of OSMRβ-deficient mice (suppl. Fig. 2h-j), when curves converged. In summary, these data indicate that OSM does not modulate the peripheral myelin-specific T cell response, but rather affects pathogenic T cell infiltration into the inflamed CNS.

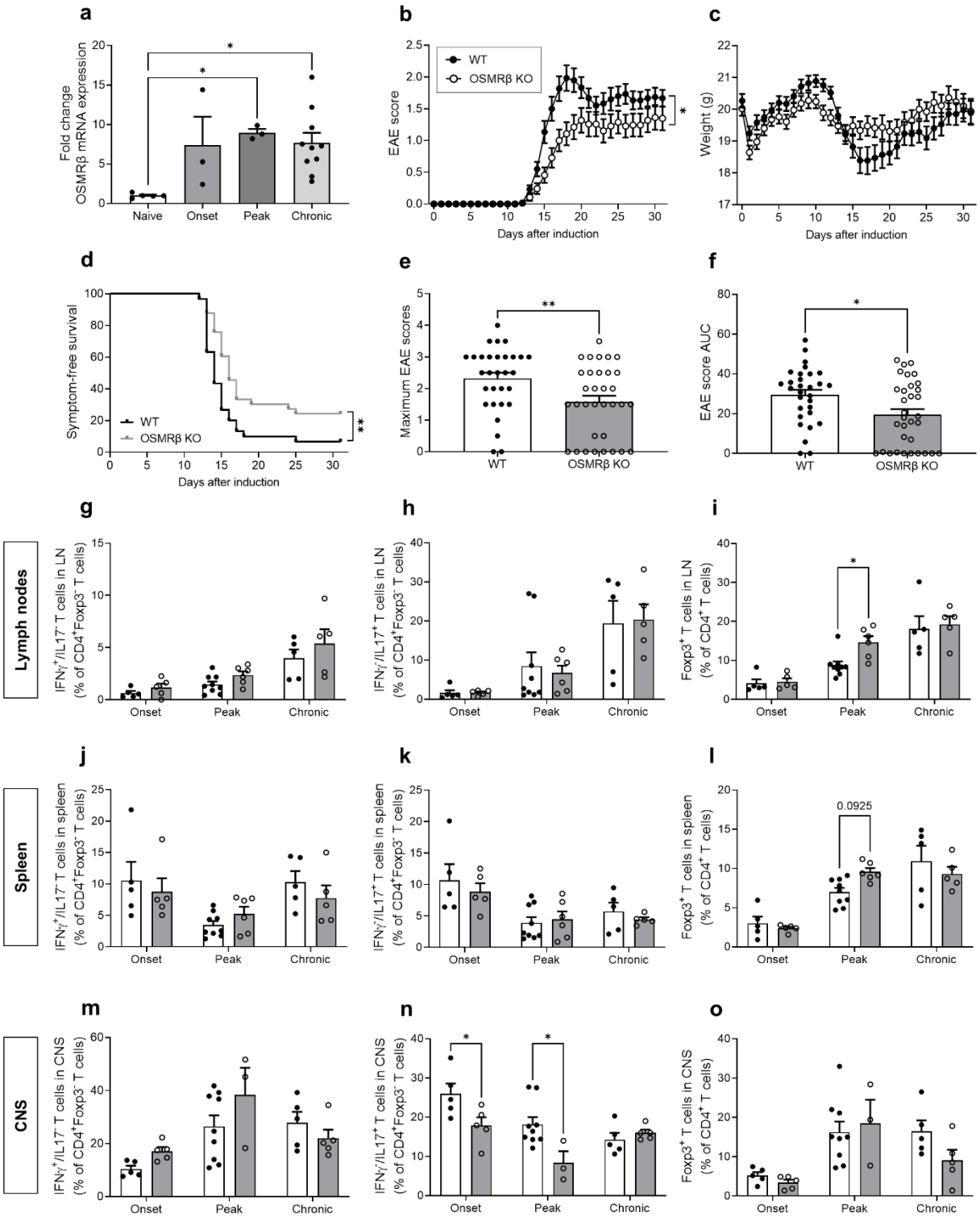


**Fig. 3** Milder course of EAE in OSMRβ-deficient mice is associated with less Th17 cell infiltration. WT and OSMRβ KO mice were injected with $MOG_{35-55}$ in CFA and 40 ng/100 µl PTX. **(a)** OSMRβ mRNA levels in CNS of WT mice at onset (n=3), peak (n=3) and chronic phase of EAE (n=10) compared to naïve mice (n=5). **(b)** Daily clinical scores and **(c)** weights were measured (WT: n=30; OSMRβ KO: n=33; pooled data of 3 independent experiments). **(d)** Kaplan-Meier curve of symptom-free survival. **(e)** Maximum EAE scores and **(f)** AUC of EAE scores were analysed. Mice were sacrificed at onset (13 dpi; WT: n=5; KO: n=5), peak (19 dpi; WT: n=9; KO: n=3-6) and chronic phase of EAE (50 dpi; WT: n=5; KO: n=5). White and grey bars depict WT and OSMRβ KO mice, respectively. **(g, j, m)** Flow cytometric analysis of the percentage of $IFN\gamma^+/IL17^-$ $CD4^+$ T cells, **(h, k, n)** $IFN\gamma^-/IL17^+$ $CD4^+$ T cells and **(i, l, o)** $Foxp3^+$ Tregs in lymph nodes, spleen and CNS, respectively. Statistical analysis was performed using Mann-Whitney test or two-way ANOVA and Šidák's multiple comparisons test with *p≤0.05, **p≤0.01. Data are

depicted as mean ± SEM. EAE, experimental autoimmune encephalomyelitis; WT, wild type; OSMRβ KO, oncostatin M receptor knock-out; AUC, area under curve; LN, lymph nodes; IFNγ, interferon gamma; IL17, interleukin 17.

## OSM signaling impairs BBB integrity via downregulation of claudin-5 and VE-cadherin

To identify the mechanism behind the decreased Th17 cell infiltration in the CNS of OSMRβ-deficient EAE mice, we first examined the effect of OSM signaling on BBB integrity. Spinal cord tissue analysis was performed in WT and OSMRβ-deficient naive mice and at EAE onset, peak and the chronic phase of disease. *In vivo* BBB leakage was visualized by staining for endogenous IgG antibodies and the laminin basement membrane of the blood vessels (Fig. 4a, b). We found that IgG leakage into the parenchyma was significantly reduced in OSMRβ KO mice at peak and in the chronic phase of disease, compared to WT mice (Fig. 4a). These data are in line with the clinical disease course (Fig. 3b) and indicate that the milder EAE symptoms in mice that lack OSMRβ signaling is at least in part due to reduced BBB leakage in the spinal cord parenchyma.

To elucidate the molecular mechanism causing reduced BBB integrity, we first validated the expression of OSMRβ on murine and human BBB-ECs. OSMRβ mRNA expression is increased upon inflammation in human and mouse BBB-ECs. In addition, OSM can induce its own receptor and has an additive effect when combined with inflammation in human BBB-ECs (Fig. 4c, d). Subsequently, we studied the effect of OSM on BBB integrity *in vitro*, by measuring the TEER across resting and inflamed BBB-ECs. In BBB-ECs from both mouse and human origin, OSM decreased TEER values to the same extent as inflammatory stimuli, TNFα and IFNγ, alone or in combination (Fig. 4e, h). This effect was abrogated in OSMRβ-deficient MBMECs (Suppl. Fig. 3a). The decreased barrier resistance was reflected by a significantly reduced protein expression of claudin-5 (Fig. 4f, g, i) and VE-cadherin (Fig. 4j), quantified by western blot and flow cytometry, respectively. Altogether, these data indicate that OSM impairs the barrier integrity of BBB-ECs in resting and inflammatory conditions through downregulation of junctional proteins.

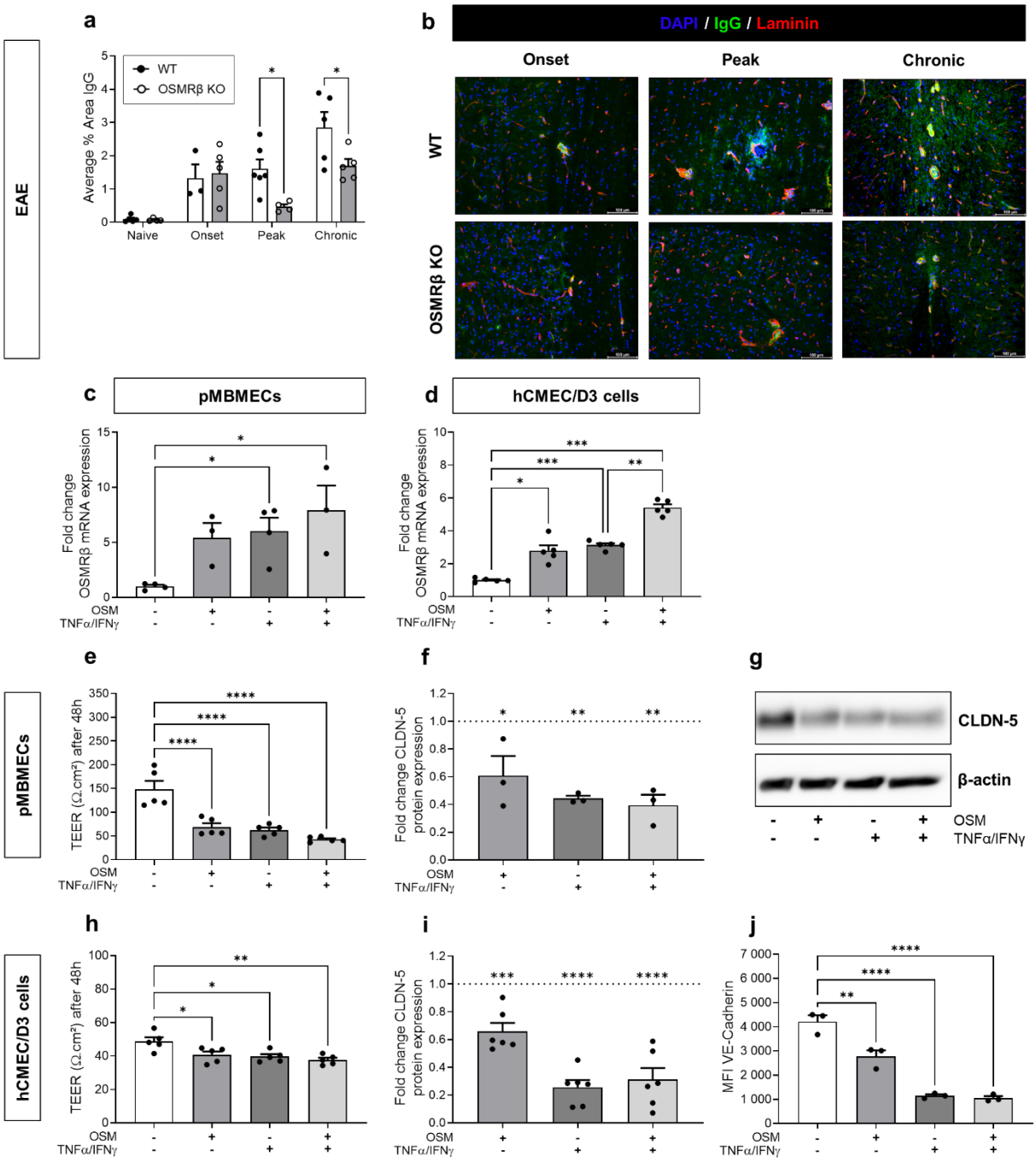


**Fig. 4** OSM signaling impairs BBB integrity *in vivo* and *in vitro* via downregulation of claudin-5 and VE-cadherin in resting and inflamed BBB-ECs. **(a)** Quantification of IgG/laminin staining in the spinal cord of naive WT and OSMRβ KO mice and at onset, peak and the chronic phase of EAE (n =3-6/group). Statistical analysis was performed using two-way ANOVA and Šidák's multiple comparisons test. **(b)** Representative images showing IgG (green) and laminin (red). Scale bars represent 100 µm. qPCR analysis of OSMRβ mRNA in **(c)** primary MBMECs (n = 3-4) and **(d)** hCMEC/D3 cells (n = 5) treated with 25 ng/ml OSM in the presence/absence of 10 ng/ml TNF-α/IFN-γ for 24h. **(e, h)** TEER was measured manually or in real-time (MBMECs: n = 5; hCMEC/D3: n = 5) after 48h stimulation. **(f, g, i)** Claudin-5 (20 kDa) expression was quantified using western blot (MBMECs: n = 3; hCMEC/D3: n = 6) and normalised to β-actin (40 kDa). **(j)** VE-Cadherin expression was analysed using flow cytometric analysis (hCMEC/D3: n = 3). Statistical analysis was performed using one-way ANOVA and Šidák's multiple comparisons test with *p≤0.05, **p≤0.01, ***p≤0.001, ***p≤0.0001. Data are depicted as mean ± SEM. EAE, experimental autoimmune encephalomyelitis; WT, wild type; OSMRβ KO, oncostatin M receptor knock-out; IgG, immunoglobulin G; TEER, transendothelial electrical resistance; CLDN-5, claudin-5; MFI: median fluorescence intensity; OSM, oncostatin M; TNFα, tumor necrosis factor alpha; IFNγ, interferon gamma.

## OSM upregulates CCL20 production by inflamed BBB-ECs and reactive astrocytes

Next to BBB integrity, we sought to determine the effect of OSM signalling on BBB-EC activation, i.e. production of chemokines and surface expression of leukocyte adhesion molecules, since these processes also actively contribute to the immune cell migration process. First, chemokine production was measured in conditioned medium of hCMEC/D3 cells, subjected to OSM in control and inflammatory conditions. The secretion of 31 chemokines was investigated using a human chemokine array as semi-quantitative method. The normalized spot volume, relative to the internal positive control and experimental control, is depicted in Fig. 5a. Treatment with TNFα and IFNγ strongly induced the secretion of CXCL11, CCL2, CCL20, CXCL10, CXCL9 and fractalkine by human BBB-ECs, while CXCL12 was the only chemokine that was downregulated. Strikingly, CCL20, a Th17 cell-attracting chemokine, was the only chemokine that was further increased by adding OSM on top of the inflammatory stimuli, suggesting a cumulative effect. Therefore, we validated CCL20 expression and secretion using qPCR on BBB-ECs (Fig. 5b) and ELISA (Fig. 5c) on conditioned medium, respectively. Indeed, OSM significantly enhanced CCL20 production at the mRNA and protein level after treatment with TNFα and IFNγ, which was also confirmed in mouse BBB-ECs (Fig. 5c).

Since CCL20 was shown to be highly produced by choroid plexus (CP) epithelial cells and reactive astrocytes in the inflamed CNS [50], we questioned whether OSM has a similar enhancing effect. As expected, treatment with TNFα and IFNγ significantly upregulated CCL20 secretion in human CP epithelial cells, however, OSM did not enhance its production (Fig. 5e), as it did in BBB-ECs. When analysing primary human and murine astrocytes, we found increased production of CCL20 by OSM, mainly in inflammatory conditions (Fig. 5f, g). These data reveal that both BBB-ECs and BBB-associated astrocytes produce CCL20 upon OSM stimulation, confirming an OSM-CCL20 axis. We validated these findings *in situ*, where CCL20 was highly produced at sites of cell infiltration with a clear vasculature-related staining, showing a trend towards CCL20 downregulation in the spinal cord of OSMRβ KO EAE mice at peak of disease (Fig. 5h, i). Finally, we found clear CCL20 expression both in BBB-ECs and astrocytes within post-mortem MS lesions (Fig. 5j, k). In conclusion, OSM promotes the secretion of CCL20 by inflamed BBB-ECs and reactive astrocytes, which potentially affects leukocyte migration across the BBB.

## OSM downregulates leukocytes adhesion molecule expression on inflamed BBB-ECs

As a second measure of BBB activation, primary mouse and human BMECs and the hCMEC/D3 cell line were subjected to OSM in control and inflammatory conditions, after which ICAM-1 and VCAM-1 expression was measured using flow cytometry. As expected, stimulation with TNFα and IFNγ significantly enhanced ICAM-1 and VCAM-1 expression in all cell types, while OSM alone did not change their expression compared to control BBB-ECs (Fig. 6a-f). In contrast to our other findings, suggesting an enhanced activation of BBB-ECs due to OSM treatment, OSM significantly decreased ICAM-1 and VCAM-1 expression in mouse BBB-ECs (Fig. 6a, d), and VCAM-1 expression in human BBB-ECs (Fig. 5e, f) in inflammatory conditions. This effect was absent in OSMRβ KO mouse derived BBB-ECs (Suppl. Fig. 3b, c). In line with this, in the CNS of EAE mice, we found that OSMRβ deficiency is associated with increased ICAM-1 and VCAM-1 mRNA expression at the chronic phase of EAE (Fig. 6g, h). Since this does not correlate with the timing of Th17 cell infiltration differences (Fig. 3n), this indicates that other mechanisms are more important for Th17 cell infiltration in OSMRβ KO mice.

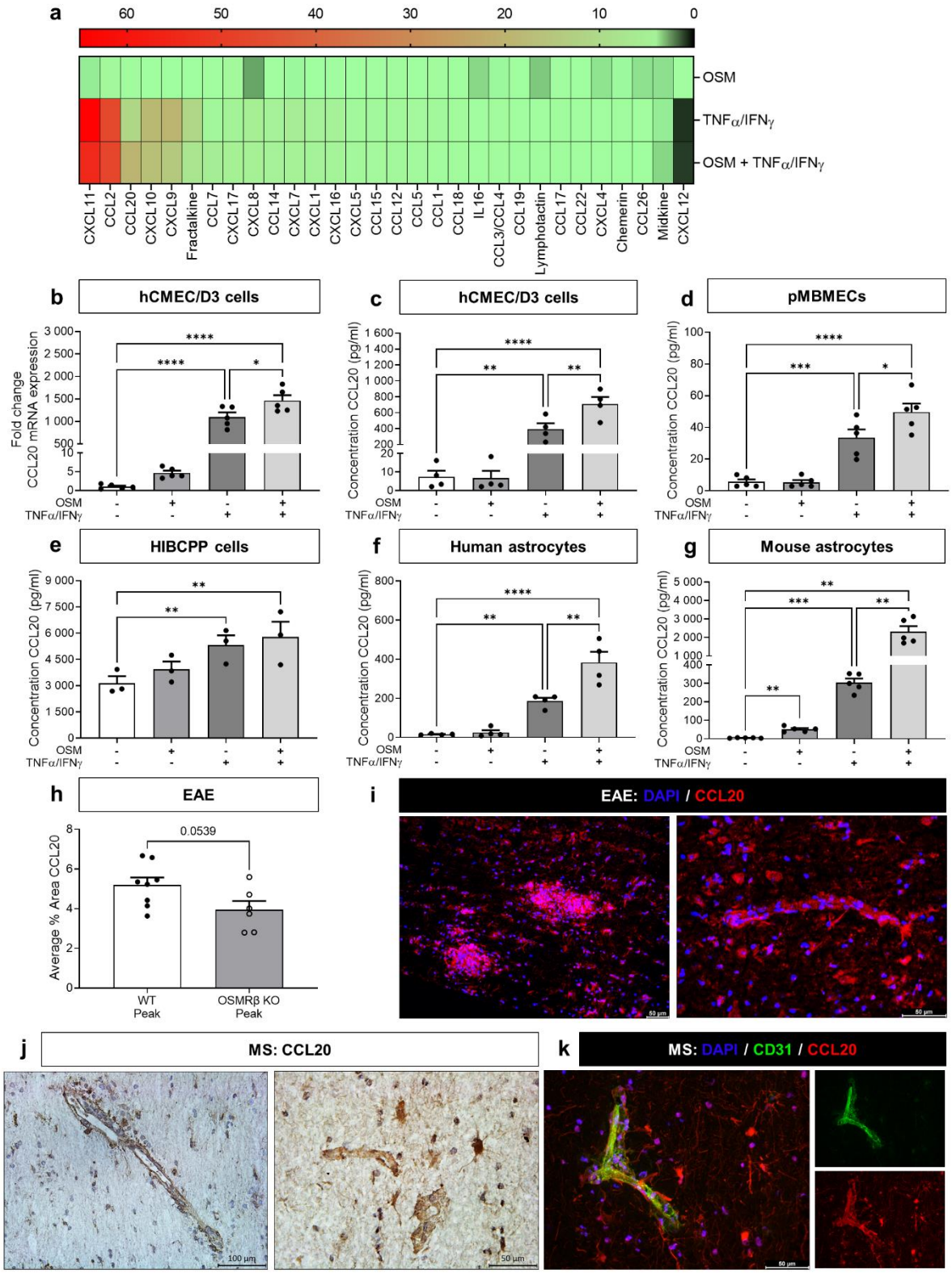


**Fig. 5** OSM upregulates CCL20 production by inflamed BBB-ECs and reactive astrocytes. **(a)** Pooled conditioned medium of 48h stimulated hCMEC/D3 cells (n = 3) was analysed using a chemokine array. Semi-quantification of the spot volume of each chemokine, relative to the internal positive control, and normalized to control medium is depicted in a heatmap. CCL20 production was validated with **(b)** qPCR in hCMEC/D3 cells (n=5) and ELISA on conditioned medium of **(c)** hCMEC/D3 cells (n = 4), **(d)** primary MBMECs (n=5), **(e)** HIBCPP choroid plexus epithelial cells (n=3), **(f)** primary human astrocytes (n=4), and **(g)** primary mouse astrocytes (n=5), treated with 25 ng/ml OSM in the presence/absence of 10 ng/ml TNF-α/IFN-γ for 48h. **(h)** Quantification of CCL20 staining in the spinal cord of WT and OSMRβ KO mice at EAE peak (n =6-8/group). **(i)** Fluorescent images showing CCL20 (red). **(j)** Immunostaining for CCL20 in active human MS lesions shows expression by blood vessel endothelial cells, as well as by astrocytes, based on morphology and proximity to blood vessels. **(k)** Immunofluorescence of

CCL20 (red) and CD31 (green, endothelial cell marker) show co-localization and astrocyte morphology. Nuclear staining was performed with DAPI (blue). Scale bars represent 50 or 100 µm. Statistical analysis was performed using one-way ANOVA with matched data and Šidák's multiple comparisons test or Mann-Whitney test with *p≤0.05, **p≤0.01, ***p≤0.001, ***p≤0.0001. Data are depicted as mean ± SEM. TNFα, tumor necrosis factor alpha; IFNγ, interferon gamma; CCL, C-C motif chemokine ligand.

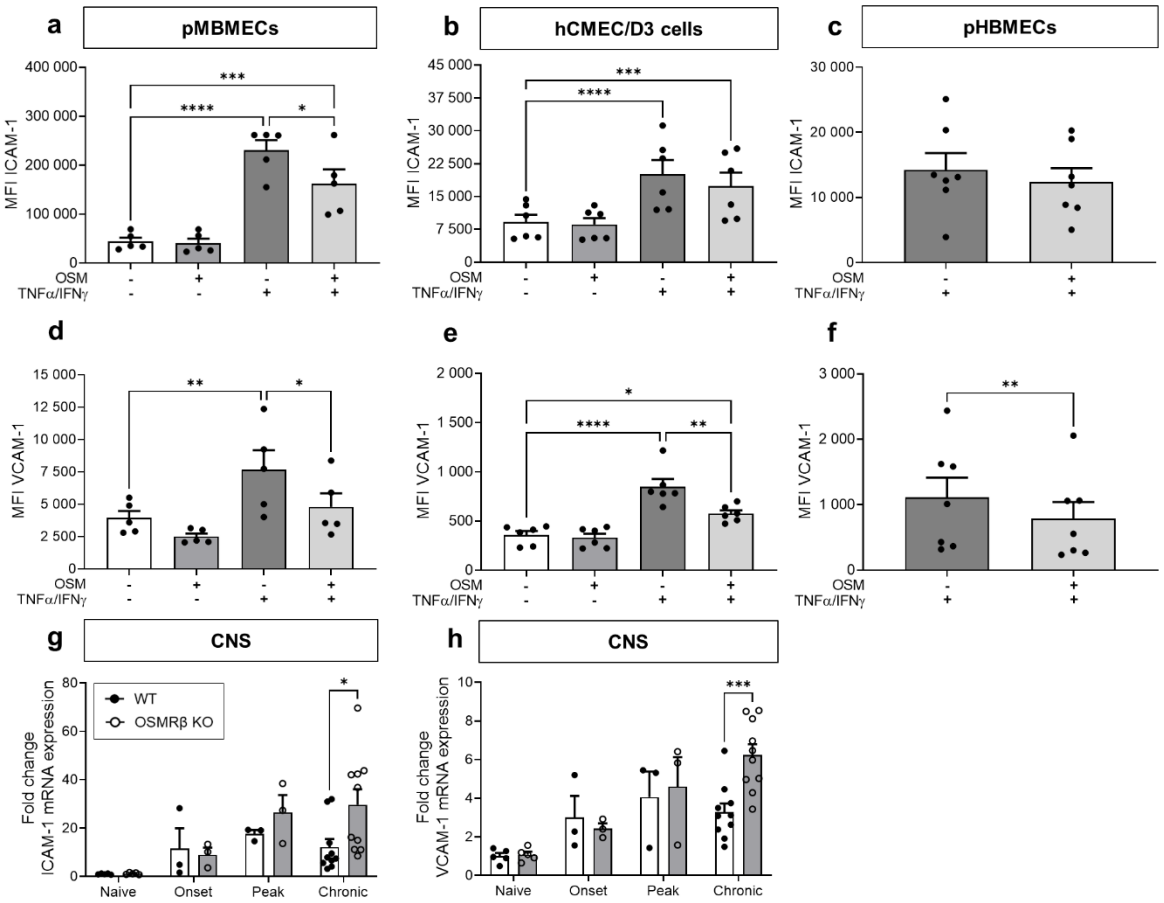


**Fig. 6** OSM downregulates ICAM-1 and VCAM-1 adhesion molecules on inflamed BBB-ECs. **(a, d)** Primary MBMECs (n = 5), **(b, e)** hCMEC/D3 cells (n = 6) and **(c, f)** primary HBMECs (n = 7) were stimulated with 25 ng/ml OSM in the presence/absence of 10 ng/ml TNF-α/IFN-γ for 48h. Flow cytometric analysis of **(a-c)** ICAM-1 and **(d-f)** VCAM-1 expression depicted as MFI. **(g)** ICAM-1 and **(h)** VCAM-1 mRNA levels in CNS of WT and OSMR KO mice at onset (n = 3), peak (n = 3) and chronic phase of EAE (n = 10) compared to naïve mice (n = 5). Statistical analysis was performed using two-way ANOVA, one-way ANOVA with matched data and Šidák's multiple comparisons test or Wilcoxon matched-pairs signed rank test with *p≤0.05, **p≤0.01, ***p≤0.001, ***p≤0.0001. Data are depicted as mean ± SEM. MFI: median fluorescence intensity; OSM, oncostatin M; ICAM-1, intercellular cell adhesion molecule 1; VCAM-1, vascular cell adhesion molecule 1; TNFα, tumor necrosis factor alpha; IFNγ, interferon gamma; WT, wild type; OSMRβ KO, oncostatin M receptor beta knock-out.

## OSM-induced endothelial CCL20 promotes Th17 cell migration mediated by integrin $\alpha_L$ activation

So far, our results show that Th17 infiltration is decreased in EAE mice that are deficient in OSM signalling, which is presumably at least in part due to changes in BBB integrity and activation. Since Th17 cell infiltration in the CNS of OSMR deficient EAE mice appears to be less CAM-dependent, we argued that these effects might be mediated by higher integrin affinity (e.g. integrin $\alpha_L$) on T cells. We examined the involvement of CCL20 in chemokine-induced integrin $\alpha_L$ activation on Th17 cells, since CCL20-mediated Th17 cell migration is ICAM-1 dependent [3, 18, 19, 40, 70]. Because integrin activation is characterized by a conformational change, we applied flow cytometric FRET (Fig. 7a) to differentiated human Th17 cells. We show that BBB-EC conditioned medium of cells treated with TNFα, IFNγ and OSM (which contains a high concentration of CCL20; Fig. 5c) significantly induced integrin αL activation, comparable to CCL20 enriched medium (Fig. 7b).

Next, we tested whether OSM, in inflammatory conditions, enhances adhesion of Th17 cells using a modified Boyden chamber assay. The number of adherent cells to the EC monolayer was quantified, showing that OSM increases adhesion of Th17 cells to inflamed BBB-ECs, compared to inflammation alone (Fig. 7c, d). In this assay, we further found that the OSM-induced effect was abrogated when ICAM-1 was blocked. Together, these results confirm that OSM, in inflammatory conditions, enhances Th17 cell adhesion *in vitro*, and that ICAM-1 is (at least partially) involved herein.

In a second assay, we wanted to further establish the link between CCL20 and Th17 adhesion. Therefore, a dynamic flow system adhesion assay was performed using OSM/TNFα/IFNγ-treated hCMEC/D3 cells. In this set-up, we confirmed that CCL20 pre-treatment enhances Th17 adhesion to BBB-ECs (Fig. 7e, f). The control Th17 cells again showed a decrease in adhesion when ICAM-1 was blocked. Interestingly, this effect was abrogated in CCL20-pretreated Th17 cells (Fig. 7e), suggesting that these cells adhere using alternative CAMs. Therefore, we examined mRNA expression of other integrin $\alpha_L$ ligands (with lower affinity), i.e. ICAM-2 and ICAM-3 [67]. Indeed, ICAM-2 and ICAM-3 expression levels were not affected by OSM (Suppl. Fig. 4). This confirms our hypothesis that OSM induces activation of integrin $\alpha_L$ on Th17 cells, thereby counteracting the decrease in endothelial ICAM-1.

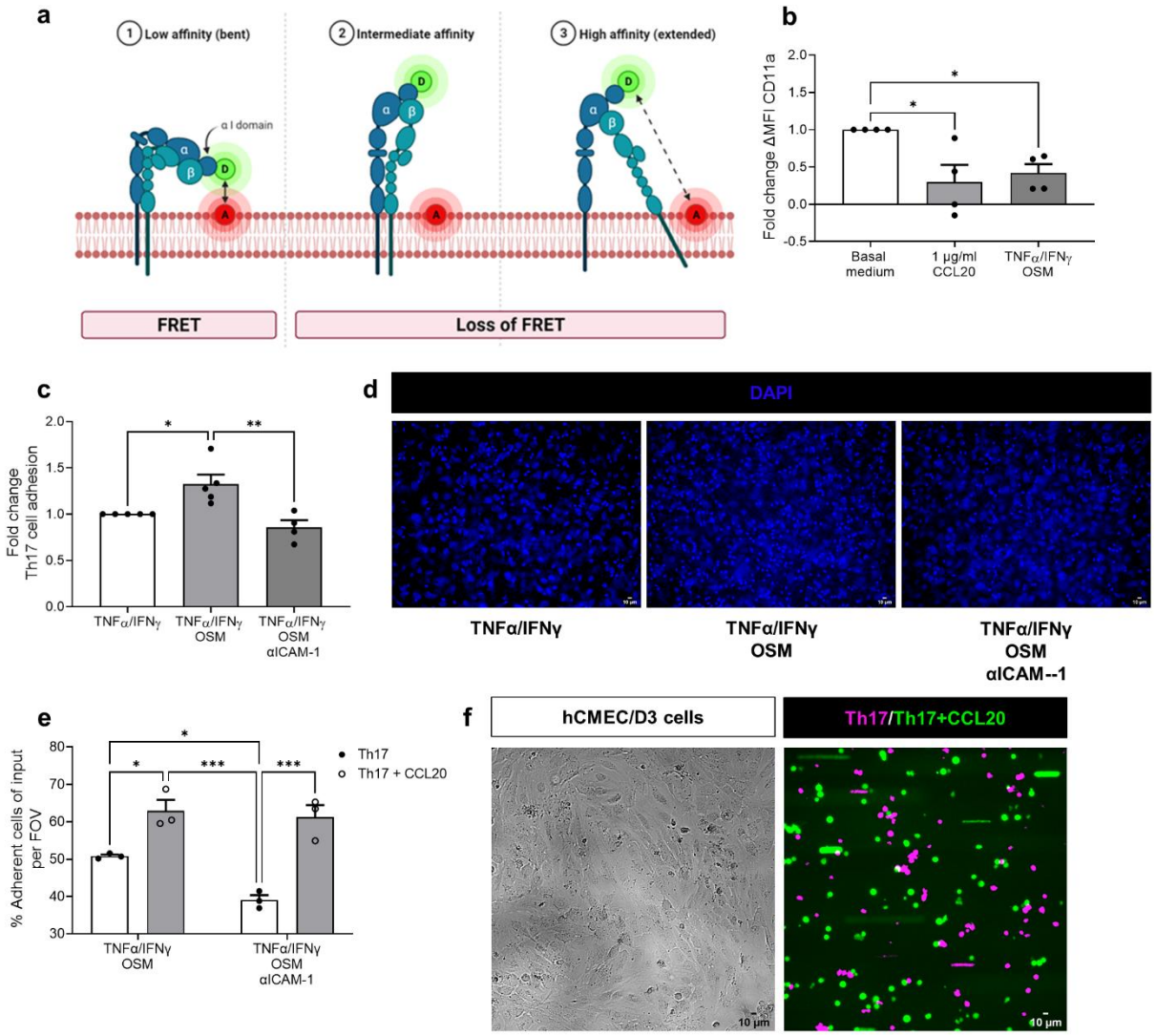


**Fig 7** OSM-induced CCL20 promotes integrin $\alpha_L$ activation and Th17 cell adhesion. **(a)** Schematic representation of FRET created with Biorender. LFA-1 is composed of $\alpha_L$-integrin (CD11a) and $\beta_2$-integrin (CD18) and has three affinity/conformation states including (1) low, (2) intermediate and (3) high. The αI domain, located in the αL integrin subunit, is responsible for ligand binding [10, 39, 67]. The αI domain of CD11 is labelled with a FITC donor (D) molecule, while the membrane is labelled with Octadecyl Rhodamine B Chloride as acceptor (A) molecule. Transfer of energy from D to A causes a decrease in the fluorescence intensity in the FITC channel, depending on the proximity of the D to A in the membrane. **(b)** The occurrence of FRET is represented as ΔMFI = $F_D$ - $F_{DA}$, where $F_D$ is the donor fluorescence in the absence of acceptor and $F_{DA}$ is the donor fluorescence in the presence of acceptor. Differentiated Th17 cells were incubated with basal medium (negative control), 1 µg/ml CCL20 enriched medium (positive control), conditioned medium of hCMEC/D3 cells treated with OSM, TNFα and IFNγ for 48h, in the presence or absence of CCL20 blocking antibody (n = 4). **(c)** Th17 cell adhesion on inflamed hCMEC/D3 cells, with or without OSM treatment and ICAM-1 blocking, normalized to the inflammatory condition. **(d)** Representative images of nuclear staining, scale bars represent 10 µm. **(e)** Dynamic flow adhesion assay of Th17 cells, with and without CCL20 pre-treatment, across OSM/TNFα/IFNγ-treated hCMEC/D3 cells, pre-incubated with an isotype control or ICAM-1 blocking antibody. Adherent cells are depicted as a percentage of total cells within the field of view (FOV). **(f)** Left shows a brightfield image hCMEC/D3 cells treated with 25 ng/ml OSM and 10 ng/ml TNFα/IFNγ for 24h, right shows Th17 cell adhesion at the end of time-lapse video, containing CellTraceCFSE labelled and Tag-it Violet labelled Th17 cells, with and without CCL20 pre-treatment, respectively. Scale bars represent 10 µm. Statistical analysis was performed using one-way ANOVA with matched data or two-way ANOVA and Šidák's multiple comparisons test with *p≤0.05, **p≤0.01. Data are depicted as mean ± SEM. MFI, median fluorescence intensity; CCL, C-C motif chemokine ligand; OSM, oncostatin M; TNFα, tumor necrosis factor alpha; IFNγ, interferon gamma; FRET, fluorescence resonance energy transfer.

## Discussion

Our research group previously demonstrated the remyelinating and neuroprotective effects of OSM in neuro-degeneration [24, 28], describing OSM as a potential therapeutic option for MS. Here, we show that OSM is highly expressed by activated myeloid cells and astrocytes in active inflammatory lesions, which is in agreement with previous reports [51, 53]. Since reactive glial cells can disturb BBB properties from inside-out [7], OSM production in the brain parenchyma complements elevated OSM levels in the blood [16, 25], being able to tackle the BBB from two sides. In addition, we found elevated OSMRβ levels in inflamed BBB-ECs and in the CNS of EAE mice, coinciding with enhanced OSM expression reported in literature [11, 22]. However, the role of OSM during neuro-inflammation remains poorly understood. In this study, we identified OSM as an inducer of BBB disruption and indirect recruiter of Th17 cells in neuro-inflammatory conditions without directly affecting the peripheral immune system.

More specifically, neuro-inflammation in the context of OSMRβ-deficiency resulted in milder EAE symptoms and a diminished Th17 cell infiltration into the CNS, which are major players in MS pathology [46]. In line with this, OSMRβ-deficiency in other chronic inflammatory disease models displays comparable *in vivo* effects, i.e. atherosclerotic OSMRβ KO mice show less severe symptoms due to reduced immune cell infiltration in atherosclerotic lesions [71]. Since no difference in the number of Th17 cells was found in peripheral organs of WT versus OSMRβ KO mice, we argued that OSMRβ deficiency reduces migration of Th17 cells across the BBB, instead of changing peripheral Th cell differentiation. Although we do not exclude effects of OSM on $CD8^+$ T cell or B cell infiltration, the $MOG_{35-55}$-induced EAE model is limited to a $CD4^+$ T cell-driven response [33].

Here, we report that OSM induces BBB disruption in resting and inflamed cells, shown by reduced TEER values due to downregulation of claudin-5 and VE-cadherin expression, two essential cell-cell junction at the BBB [38, 41, 56]. These results are in line with studies of Takata et al., showing a decreased TEER and increased permeability to sodium fluorescein when rat brain capillary ECs (RBECs) were stimulated with OSM, mediated by prolonged JAK/STAT3 signalling. This was accompanied by an altered cellular distribution of claudin-5 and ZO-1 TJs, while only claudin-5 protein expression was significantly reduced [58, 60]. Moreover, the effects seen by Takata et al. were rescued when RBECs were pre-treated with an anti-OSM antibody [60], which reflects our unaffected TEER measurements in OSMRβ KO mouse BBB-ECs and demonstrates that the induced barrier impairment is specifically mediated by OSMRβ signaling. Besides ECs, pericytes of the BBB were shown to be susceptible for OSM signalling, thereby aggravating the OSM-induced BBB impairment even more [59].

We further show that OSM induces the upregulation of the Th17-recruiting chemokine CCL20 and downregulates the Th1-attracting chemokines CXCL11, CXCL10, CXCL9 and fractalkine in inflamed BBB-ECs. CCL20, the CCR6 ligand, mediates firm adhesion and arrest of Th17 cells on inflamed endothelium in an ICAM-1-dependent manner [3, 18, 19, 40, 70]. MS patients show increased serum levels of CCL20, which is associated with disease severity [15, 25, 35]. In brain lesions, CCL20 is mainly expressed by reactive astrocytes and CP epithelial cells, another important lymphocyte entry site [5, 42, 50]. In EAE, the CCL20-CCR6-Th17 axis is shown to be crucial in disease induction [1, 37, 50, 66], while the CCL20-CCR6 axis is not involved in $CD8^+$ T cell and B cell migration into the CNS [34, 45]. In this study, we reveal that OSM boosts CCL20 production by inflamed BBB-ECs and reactive

astrocytes, thereby identifying an OSM-CCL20 axis and suggesting that both can contribute to Th17 cell recruitment during neuro-inflammation. In literature, OSM was shown to induce CCL2 and CCL21 secretion, while downregulating CCL5 expression, in various human vascular beds [21, 53, 57, 65], in contrast to what was seen in our chemokine array. However, our experiments were performed on the cell line hCMEC/D3, which is derived from human cerebral microvascular ECs and therefore most closely resembles BBB-ECs [69].

As a second measure of BBB activation, we found that OSM reduced VCAM-1 expression on mouse and human BBB-ECs, as well as ICAM-1 expression on mouse BBB-ECs, in inflammatory conditions. However, no effect on ICAM-1 expression was seen in human BBB-ECs. These results are in contrast with previous reports describing OSM-induced upregulation of ICAM-1 expression in human ECs from different vascular beds [17, 21, 53, 65]. Few effects of OSM on VCAM-1 expression were described, until recently, when Hanlon et al. showed OSM-induced downregulation of VCAM-1 expression on HUVECs [17, 21, 31, 53, 65], which corresponds to our *in vitro* findings on BBB-ECs. However, we want to highlight important differences with our experimental set-up as we examined the additive effect of OSM on TNFα/IFNγ stimulation, while most reports studied the single effect of OSM. Furthermore, we confirmed the OSM-induced changes on CAM expression in three different types of specialized BBB-ECs (primary MBMECs, HMECS, hCMEC/D3), which differ in their characteristics from peripheral (micro)vascular endothelial cells, showing the same downregulation of VCAM-1 expression [49]. Since no effects of OSM were found in mouse BBB-ECs that lack OSM signaling, it confirms the specific involvement of OSMRβ triggering in our observations. This is of interest since OSM can also signal via the LIFR in humans [14]. As similar results were obtained in human and mouse BBB-ECs, it is likely that the effects seen in human cells are attributed to OSMRβ signaling and not LIFRβ activation. Surprisingly, altered ICAM-1 and VCAM-1 expression *in vivo* was only detected at the end of EAE in OSMRβ deficient mice, suggesting that other mechanisms are more important for Th17 cell infiltration differences at disease onset and peak.

Therefore, we argued that upregulation of chemokine production, in particular CCL20, could overrule the OSM-induced effect on CAM expression, since chemokines induce integrin activation and clustering on leukocytes. Since CCL20 promotes Th17 cell migration in an ICAM-1-dependent fashion, we investigated the effect of CCL20 on LFA-1 activation [3, 18, 19, 40, 70]. LFA-1 is composed of $\alpha_L$-integrin (CD11a) and $\beta_2$-integrin (CD18) which both adapt their conformation to regulate the ligand binding affinity. LFA-1 shows three affinity states including low, intermediate and high. When transitioning from low to high affinity, the extracellular domain changes its conformation from a bent to an extended conformation which is able to bind to its ligand and transmit cytosolic signals. The αI domain, located in the αL integrin subunit, is responsible for ligand binding [10, 39, 67]. Chemokines secreted and presented by inflamed ECs trigger their G-protein coupled chemokine receptors on leukocytes leading to increased intracellular $Ca^{2+}$ levels. This inside-out signalling is critical for integrin bending and, ultimately, high affinity integrin activation which leads to ICAM-1 binding and firm adhesion to the endothelium [4, 19, 38, 67]. Using flow cytometric FRET, we show that OSM-induced endothelial CCL20 promoted αL-integrin activation on human Th17 cells. To our knowledge, we are the first to provide direct evidence of CCL20-induced LFA-1 activation. One limitation of this approach is that flow cytometric FRET is unable to distinguish between the intermediate and high affinity conformations, which warrants further investigation.

Finally, we showed that Th17 cell adhesion to inflamed BBB-ECs is facilitated by OSM, which is at least partially ICAM-1 mediated. Indeed, OSM was previously shown to induce leukocyte rolling and adhesion on HUVECs, having similar effects as TNFα stimulation [31]. In addition, CCL20 pre-treatment further enhanced Th17 cell adhesion under *in vitro* flow conditions, however, making them less responsive to ICAM-1. Therefore, we further hypothesize that the CCL20-induced integrin activation alternatively promotes interactions with lower affinity ligands, such as ICAM-2 or ICAM-3 [67]. In this context, ICAM-2 is an established player in T cell migration across the BBB, exerting similar functions as ICAM-1 in adhesion, arrest and crawling of Th17 cells, which could potentiate OSM-induced CCL20-mediated migration [20, 38, 41].

In conclusion, this study identifies an OSM-CCL20-Th17 cell axis and emphasizes a dual role of OSM in MS pathology. While OSM promotes remyelination during neuro-degeneration, it impairs BBB function and triggers Th17 cell infiltration during neuro-inflammation. This research triggers new questions on the effect of OSM on the infiltration of $CD8^+$ T cells and B cells, since these could not be investigated in our EAE model. Furthermore, OSM effects on other CNS cells that are important in regulating immune cell entry, such as CP epithelial cells and BBB-associated astrocytes, are interesting to study in the future. Nevertheless, our findings are of particular importance when OSM is considered as a treatment option for MS because of its neuroprotective and remyelination-enhancing properties. This study indicates the importance of investigating all possible effects of a proposed therapy, to anticipate the potential harmful side effects, in this case promoting Th17 cell entry which can trigger disease activity in MS patients [2].

## Supplementary figures

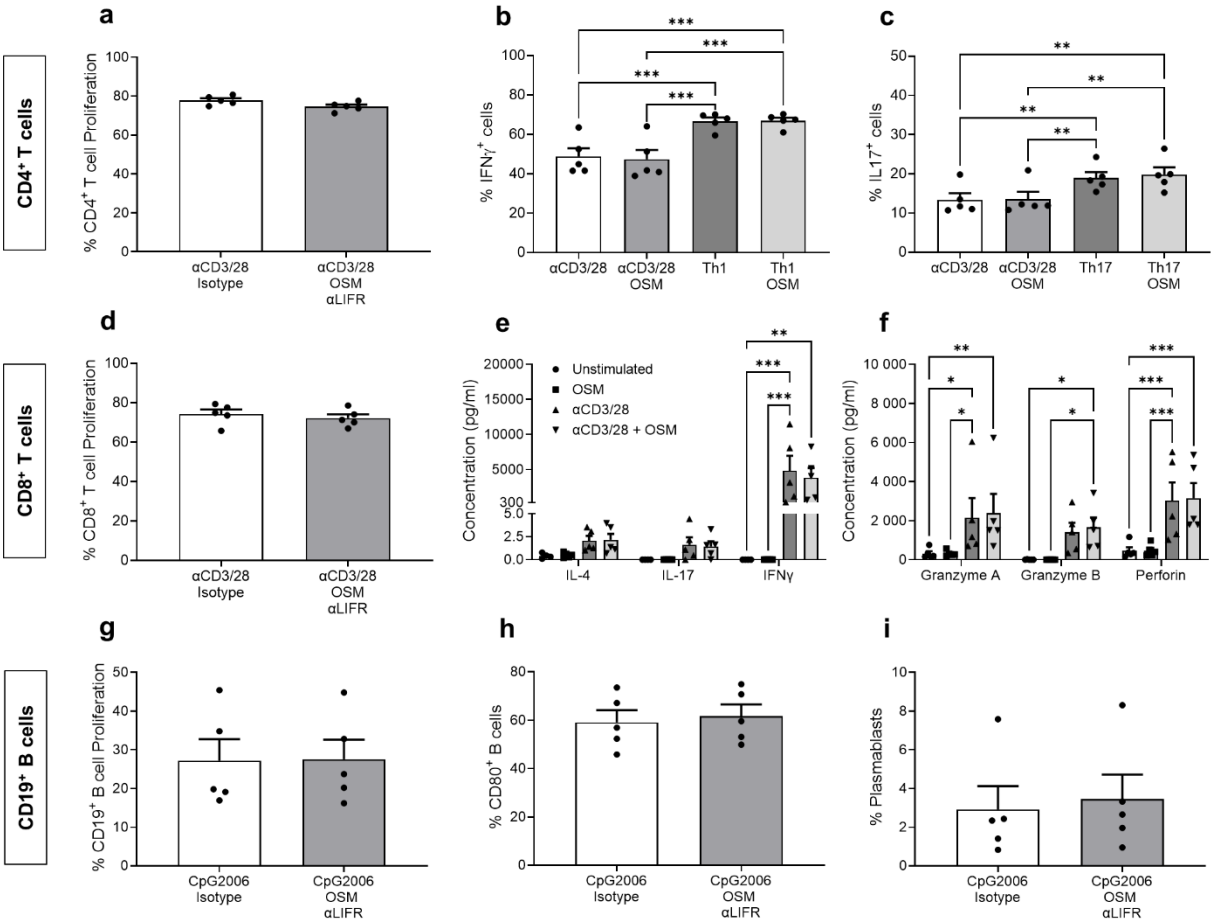


**Suppl. Fig. 1** OSM does not affect the functional properties of activated CD4⁺ T cells, CD8⁺ T cells and CD19⁺ B cells. CD4⁺ T cells, CD8⁺ T cells and B cells were isolated from PBMCs of healthy donors using magnetic selection (n=5). **(a, d, g)** T and B cell proliferation were analysed with flow cytometry after 6 days of stimulation with αCD3/28/2-coated beads or CpG2006, respectively, in the absence or presence of OSM (25 ng/ml) and anti-LIFR antibody (20 µg/ml). **(b, c)** Flow cytometric analysis of IFNγ and IL17 expression by CD4⁺ T memory cells cultured under non-skewing and Th1 or Th17 skewing conditions in the presence or absence of OSM. **(e, f)** Concentration IL4, IL17, IFNγ, granzyme A, granzyme B and perforin in the conditioned medium of resting or stimulated CD8⁺ T cells, in the absence or presence of OSM and anti-LIFR antibody, measured using LegendPlex™ multiplex assay. **(h, i)** Flow cytometric analysis of the percentage CD80⁺ activated B cells and CD24⁻CD38⁺ plasmablasts, respectively, in the absence or presence of OSM and anti-LIFR antibody. Data are depicted as mean ± SEM. Statistical analysis was performed using Wilcoxon test, one-way ANOVA and two-way ANOVA using Tukey's multiple comparisons test with *p≤0.05, **p≤0.01, ***p≤0.001. OSM, oncostatin M; LIFR, leukemia inhibitory factor; IFNγ, interferon gamma; IL, interleukin.

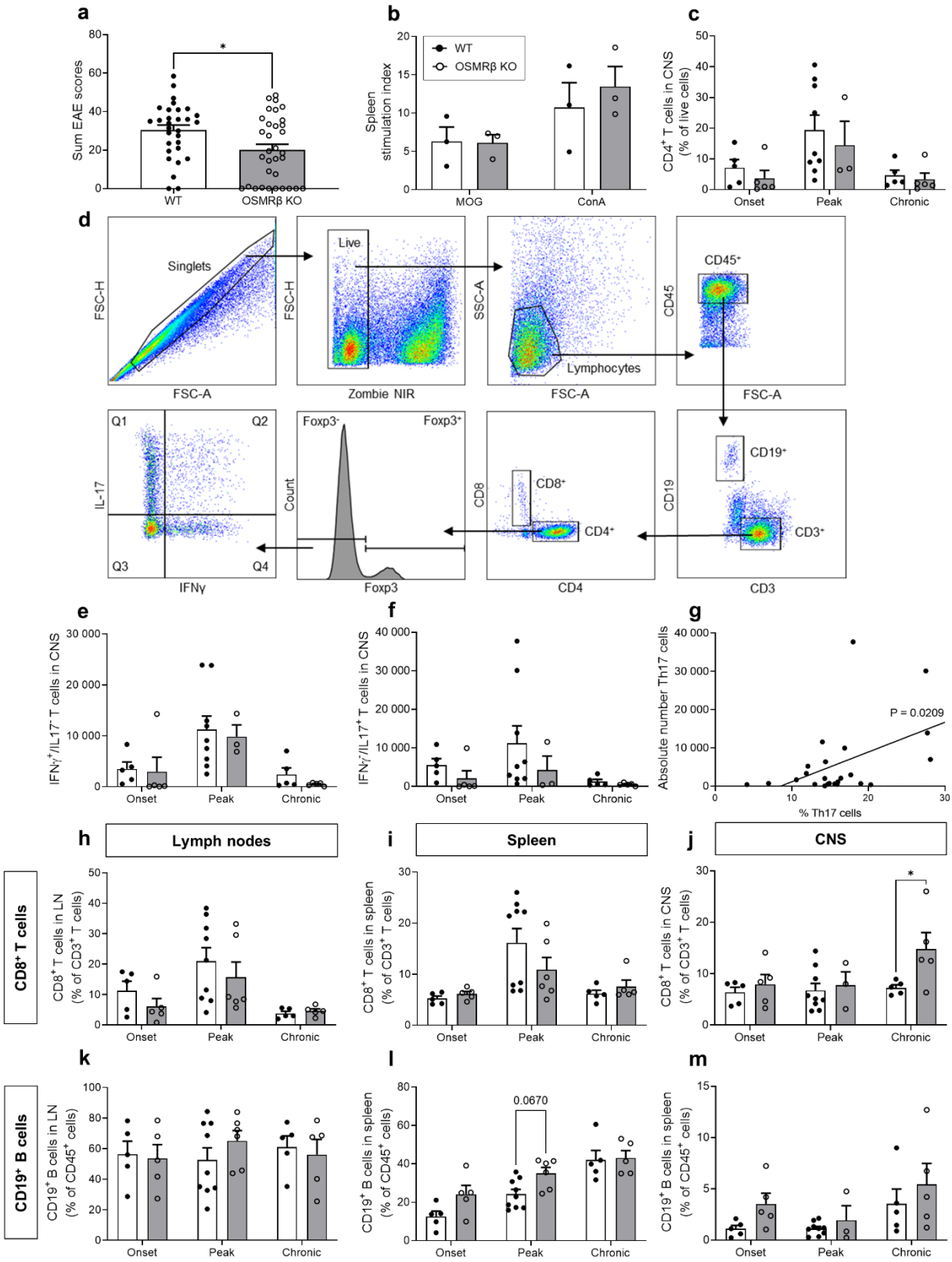


**Suppl. Fig. 2** Less severe EAE in OSMRβ-deficient mice is not attributable to an altered peripheral immune cell response. WT and OSMRβ KO mice were injected with $MOG_{35-55}$ in CFA and 40 ng/100 µl PTX (WT: n=30; OSMRβ KO: n=33; pooled data of 3 independent experiments). Mice were sacrificed at onset (13 dpi; WT: n=5; KO: n=5), peak (19 dpi; WT: n=9; KO: n=6) and chronic phase of EAE (50 dpi; WT: n=5; KO: n=5). **(a)** Sum of EAE scores were evaluated. **(b)** Lymphocyte proliferation in response to MOG or ConA as measured by CFSE incorporation in splenocytes from WT and OSMRβ KO mice, 10 days after EAE induction (n=3/genotype). **(c)** Flow cytometric analysis of the percentage of $CD4^+$ T cells within the live cell population. White and grey bars depict WT and OSMRβ KO mice, respectively. **(d)** Gating strategy of the immune cell profile in the CNS at EAE peak. Single cells are gated, using the area and height of the forward scatter (FSC-A, FSC-H). Dead cells are excluded

using Zombie NIR. Lymphocytes are gated based on forward and sideward scatter (FSC-A, SSC-A). Next, leukocytes are characterized based on CD45. T and B cells are distinguished based on CD3 and CD19, respectively. Within the $CD3^+$ T cell gate, $CD4^+$ T helper cells and $CD8^+$ cytotoxic T cells are identified. Finally, IFNγ, IL17 and Foxp3 are used to gate Th1 (Q4), Th17 (Q1) and T regulatory cells, respectively. **(e,f)** Absolute numbers of infiltrating Th1 and Th17 cells, respectively, were calculated by multiplying the percentage cells within the lymphocyte gate by the total amount of CNS-infiltrating cells, counted by an automated cell counter. **(g)** Positive correlation between % Th17 cells and absolute number of Th17 cells in pooled WT and OSMR KO mice (EAE score > 0), using simple linear regression. **(h-m)** Flow cytometric analysis of the percentage of $CD8^+$ T cells and $CD19^+$ B cells in lymph nodes, spleen and CNS, respectively. Statistical analysis was performed using two-way ANOVA and Sidak's multiple comparisons test. Data are depicted as mean ± SEM. EAE, experimental autoimmune encephalomyelitis; MOG, myelin oligodendrocyte glycoprotein; ConA, Concanavalin A; WT, wild type; OSMRβ KO, oncostatin M receptor knock-out; IFNγ, interferon gamma; IL17, interleukin 17; Th, T helper cell.

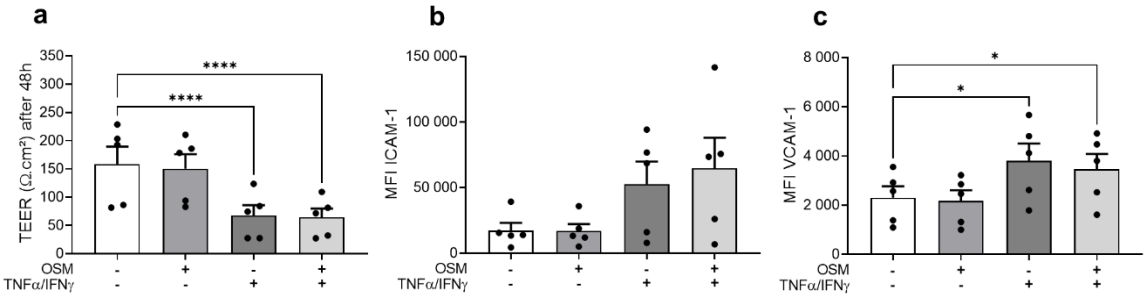


**Suppl. Fig. 3** OSM-induced effects on mouse BBB-ECs are abrogated in absence of OSMRβ signaling. Primary MBMECs isolated from OSMRβ KO mice (n=5) were treated with 25 ng/ml OSM in the presence/absence of 10 ng/ml TNF-α/IFN-γ for 48h. **(a)** TEER was measured manually. Flow cytometric analysis of **(b)** ICAM-1 and **(c)** VCAM-1 expression depicted as median fluorescence intensity (MFI). Statistical analysis was performed using one-way ANOVA with matched data and Šidák's multiple comparisons test with *p≤0.05, **p≤0.01, ***p≤0.001, ***p≤0.0001. Data are depicted as mean ± SEM. MFI: median fluorescence intensity; OSM, oncostatin M; ICAM-1, intercellular cell adhesion molecule 1; VCAM-1, vascular cell adhesion molecule 1; TNFα, tumor necrosis factor alpha; IFNγ, interferon gamma; TEER, transendothelial electrical resistance.

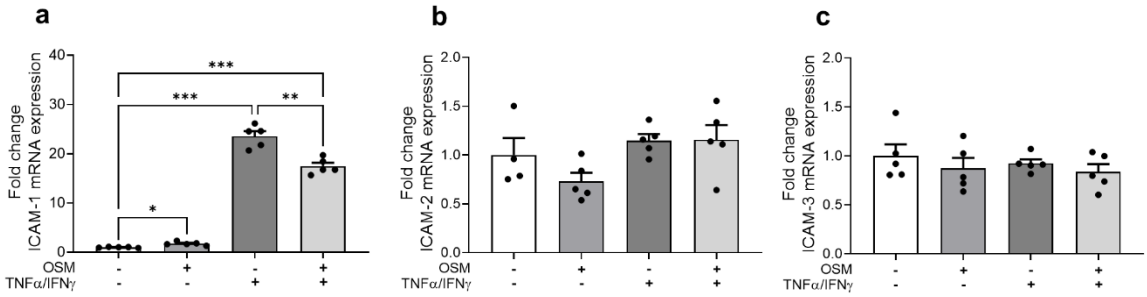


**Suppl. Fig. 4** ICAM-2 and ICAM-3 expression is not affected by OSM treatment. qPCR analysis of **(a)** ICAM-1, **(b)** ICAM-2 and **(c)** ICAM-3 OSMRβ mRNA hCMEC/D3 cells (n = 5) treated with 25 ng/ml OSM in the presence/absence of 10 ng/ml TNF-α/IFN-γ for 24h. Statistical analysis was performed using one-way ANOVA and Šidák's multiple comparisons test with *p≤0.05, **p≤0.01, ***p≤0.001, ***p≤0.0001. Data are depicted as mean ± SEM. OSM, oncostatin M; TNFα, tumor necrosis factor alpha; IFNγ, interferon gamma; ICAM, intercellular cell adhesion molecule.

## References


1. Abraham M, Karni A, Mausner-Fainberg K, Weiss ID and Peled A. (2017) Natural and induced immunization against CCL20 ameliorate experimental autoimmune encephalitis and may confer protection against multiple sclerosis. Clin Immunol 183:316-24. https://doi.org/10.1016/j.clim.2017.09.018
2. Akgün K, Blankenburg J, Marggraf M, Haase R and Ziemssen T. (2020) Event-Driven Immunoprofiling Predicts Return of Disease Activity in Alemtuzumab-Treated Multiple Sclerosis. Front Immunol 11:56. https://doi.org/10.3389/fimmu.2020.00056
3. Alcaide P, Maganto-Garcia E, Newton G, Travers R, Croce KJ, Bu DX, Luscinskas FW and Lichtman AH. (2012) Difference in Th1 and Th17 lymphocyte adhesion to endothelium. J Immunol 188(3):1421-30. https://doi.org/10.4049/jimmunol.1101647
4. Alon R and Shulman Z. (2011) Chemokine triggered integrin activation and actin remodeling events guiding lymphocyte migration across vascular barriers. Exp Cell Res 317(5):632-41. https://doi.org/10.1016/j.yexcr.2010.12.007
5. Ambrosini E, Remoli ME, Giacomini E, Rosicarelli B, Serafini B, Lande R, Aloisi F and Coccia EM. (2005) Astrocytes produce dendritic cell-attracting chemokines in vitro and in multiple sclerosis lesions. J Neuropathol Exp Neurol 64(8):706-15. https://doi.org/10.1097/01.jnen.0000173893.01929.fc
6. Benson K, Cramer S and Galla HJ. (2013) Impedance-based cell monitoring: barrier properties and beyond. Fluids Barriers CNS 10(1):5. https://doi.org/10.1186/2045-8118-10-5
7. Broux B, Gowing E and Prat A. (2015) Glial regulation of the blood-brain barrier in health and disease. Semin Immunopathol 37(6):577-90. https://doi.org/10.1007/s00281-015-0516-2
8. Broux B, Zandee S, Gowing E, Charabati M, Lécuyer MA, Tastet O, Hachehouche L, Bourbonnière L, Ouimet JP, Lemaitre F, Larouche S, Cayrol R, Bouthillier A, Moumdjian R, Lahav B, Poirier J, Duquette P, Arbour N, Peelen E and Prat A. (2020) Interleukin-26, preferentially produced by T(H)17 lymphocytes, regulates CNS barrier function. Neurol Neuroimmunol Neuroinflamm 7(6). https://doi.org/10.1212/nxi.0000000000000870
9. Chen SH and Benveniste EN. (2004) Oncostatin M: a pleiotropic cytokine in the central nervous system. Cytokine Growth Factor Rev 15(5):379-91. https://doi.org/10.1016/j.cytogfr.2004.06.002
10. Chigaev A, Smagley Y, Haynes MK, Ursu O, Bologa CG, Halip L, Oprea T, Waller A, Carter MB, Zhang Y, Wang W, Buranda T and Sklar LA. (2015) FRET detection of lymphocyte function-associated antigen-1 conformational extension. Mol Biol Cell 26(1):43-54. https://doi.org/10.1091/mbc.E14-06-1050
11. Deerhake ME, Danzaki K, Inoue M, Cardakli ED, Nonaka T, Aggarwal N, Barclay WE, Ji RR and Shinohara ML. (2021) Dectin-1 limits autoimmune neuroinflammation and promotes myeloid cell-astrocyte crosstalk via Card9-independent expression of Oncostatin M. Immunity 54(3):484-98.e8. https://doi.org/10.1016/j.immuni.2021.01.004
12. Dendrou CA, Fugger L and Friese MA. (2015) Immunopathology of multiple sclerosis. Nat Rev Immunol 15(9):545-58. https://doi.org/10.1038/nri3871
13. Dhaeze T, Tremblay L, Lachance C, Peelen E, Zandee S, Grasmuck C, Bourbonnière L, Larouche S, Ayrignac X, Rébillard RM, Poirier J, Lahav B, Duquette P, Girard M, Moumdjian R, Bouthillier A, Larochelle C and Prat A. (2019) CD70 defines a subset of proinflammatory and CNS-pathogenic T(H)1/T(H)17 lymphocytes and is overexpressed in multiple sclerosis. Cell Mol Immunol 16(7):652-65. https://doi.org/10.1038/s41423-018-0198-5
14. Drechsler J, Grötzinger J and Hermanns HM. (2012) Characterization of the rat oncostatin M receptor complex which resembles the human, but differs from the murine cytokine receptor. PLoS One 7(8):e43155. https://doi.org/10.1371/journal.pone.0043155
15. El Sharkawi FZ, Ali SA, Hegazy MI and Atya HB. (2019) The combined effect of IL-17F and CCL20 gene polymorphism in susceptibility to multiple sclerosis in Egypt. Gene 685:164-9. https://doi.org/10.1016/j.gene.2018.11.006
16. Ensoli F, Fiorelli V, Lugaresi A, Farina D, De Cristofaro M, Collacchi B, Muratori DS, Scala E, Di Gioacchino M, Paganelli R and Aiuti F. (2002) Lymphomononuclear cells from multiple sclerosis patients spontaneously produce high levels of oncostatin M, tumor necrosis factors alpha and beta, and interferon gamma. Mult Scler 8(4):284-8. https://doi.org/10.1191/1352458502ms817oa
17. Fearon U, Mullan R, Markham T, Connolly M, Sullivan S, Poole AR, FitzGerald O, Bresnihan B and Veale DJ. (2006) Oncostatin M induces angiogenesis and cartilage degradation in rheumatoid arthritis synovial tissue and human cartilage cocultures. Arthritis Rheum 54(10):3152-62. https://doi.org/10.1002/art.22161
18. Fitzhugh DJ, Naik S, Caughman SW and Hwang ST. (2000) Cutting edge: C-C chemokine receptor 6 is essential for arrest of a subset of memory T cells on activated dermal microvascular endothelial cells under physiologic flow conditions in vitro. J Immunol 165(12):6677-81. https://doi.org/10.4049/jimmunol.165.12.6677

19. Ghannam S, Dejou C, Pedretti N, Giot JP, Dorgham K, Boukhaddaoui H, Deleuze V, Bernard FX, Jorgensen C, Yssel H and Pène J. (2011) CCL20 and β-defensin-2 induce arrest of human Th17 cells on inflamed endothelium in vitro under flow conditions. J Immunol 186(3):1411-20. https://doi.org/10.4049/jimmunol.1000597
20. Haghayegh Jahromi N, Marchetti L, Moalli F, Duc D, Basso C, Tardent H, Kaba E, Deutsch U, Pot C, Sallusto F, Stein JV and Engelhardt B. (2019) Intercellular Adhesion Molecule-1 (ICAM-1) and ICAM-2 Differentially Contribute to Peripheral Activation and CNS Entry of Autoaggressive Th1 and Th17 Cells in Experimental Autoimmune Encephalomyelitis. Front Immunol 10:3056. https://doi.org/10.3389/fimmu.2019.03056
21. Hanlon MM, Rakovich T, Cunningham CC, Ansboro S, Veale DJ, Fearon U and McGarry T. (2019) STAT3 Mediates the Differential Effects of Oncostatin M and TNFα on RA Synovial Fibroblast and Endothelial Cell Function. Front Immunol 10:2056. https://doi.org/10.3389/fimmu.2019.02056
22. Haroon F, Drögemüller K, Händel U, Brunn A, Reinhold D, Nishanth G, Mueller W, Trautwein C, Ernst M, Deckert M and Schlüter D. (2011) Gp130-dependent astrocytic survival is critical for the control of autoimmune central nervous system inflammation. J Immunol 186(11):6521-31. https://doi.org/10.4049/jimmunol.1001135
23. Houben E, Hellings N and Broux B. (2019) Oncostatin M, an Underestimated Player in the Central Nervous System. Front Immunol 10:1165. https://doi.org/10.3389/fimmu.2019.01165
24. Houben E, Janssens K, Hermans D, Vandooren J, Van den Haute C, Schepers M, Vanmierlo T, Lambrichts I, van Horssen J, Baekelandt V, Opdenakker G, Baron W, Broux B, Slaets H and Hellings N. (2020) Oncostatin M-induced astrocytic tissue inhibitor of metalloproteinases-1 drives remyelination. Proc Natl Acad Sci U S A 117(9):5028-38. https://doi.org/10.1073/pnas.1912910117
25. Huang J, Khademi M, Fugger L, Lindhe Ö, Novakova L, Axelsson M, Malmeström C, Constantinescu C, Lycke J, Piehl F, Olsson T and Kockum I. (2020) Inflammation-related plasma and CSF biomarkers for multiple sclerosis. Proc Natl Acad Sci U S A 117(23):12952-60. https://doi.org/10.1073/pnas.1912839117
26. Ichihara M, Hara T, Kim H, Murate T and Miyajima A. (1997) Oncostatin M and leukemia inhibitory factor do not use the same functional receptor in mice. Blood 90(1):165-73.
27. Ishiwata I, Ishiwata C, Ishiwata E, Sato Y, Kiguchi K, Tachibana T, Hashimoto H and Ishikawa H. (2005) Establishment and characterization of a human malignant choroids plexus papilloma cell line (HIBCPP). Hum Cell 18(1):67-72. https://doi.org/10.1111/j.1749-0774.2005.tb00059.x
28. Janssens K, Maheshwari A, Van den Haute C, Baekelandt V, Stinissen P, Hendriks JJ, Slaets H and Hellings N. (2015) Oncostatin M protects against demyelination by inducing a protective microglial phenotype. Glia 63(10):1729-37. https://doi.org/10.1002/glia.22840
29. Janssens K, Van den Haute C, Baekelandt V, Lucas S, van Horssen J, Somers V, Van Wijmeersch B, Stinissen P, Hendriks JJ, Slaets H and Hellings N. (2015) Leukemia inhibitory factor tips the immune balance towards regulatory T cells in multiple sclerosis. Brain Behav Immun 45:180-8. https://doi.org/10.1016/j.bbi.2014.11.010
30. Jones SA and Jenkins BJ. (2018) Recent insights into targeting the IL-6 cytokine family in inflammatory diseases and cancer. Nat Rev Immunol 18(12):773-89. https://doi.org/10.1038/s41577-018-0066-7
31. Kerfoot SM, Raharjo E, Ho M, Kaur J, Serirom S, McCafferty DM, Burns AR, Patel KD and Kubes P. (2001) Exclusive neutrophil recruitment with oncostatin M in a human system. Am J Pathol 159(4):1531-9. https://doi.org/10.1016/s0002-9440(10)62538-2
32. Larochelle C, Cayrol R, Kebir H, Alvarez JI, Lécuyer MA, Ifergan I, Viel É, Bourbonnière L, Beauseigle D, Terouz S, Hachehouche L, Gendron S, Poirier J, Jobin C, Duquette P, Flanagan K, Yednock T, Arbour N and Prat A. (2012) Melanoma cell adhesion molecule identifies encephalitogenic T lymphocytes and promotes their recruitment to the central nervous system. Brain 135(Pt 10):2906-24. https://doi.org/10.1093/brain/aws212
33. Lassmann H and Bradl M. (2017) Multiple sclerosis: experimental models and reality. Acta Neuropathol 133(2):223-44. https://doi.org/10.1007/s00401-016-1631-4
34. Lee DSW, Yam JY, Grasmuck C, Dasoveanu D, Michel L, Ward LA, Rojas OL, Zandee S, Bourbonnière L, Ramaglia V, Bar-Or A, Prat A and Gommerman JL. (2021) CCR6 Expression on B Cells Is Not Required for Clinical or Pathological Presentation of MOG Protein-Induced Experimental Autoimmune Encephalomyelitis despite an Altered Germinal Center Response. J Immunol 207(6):1513-21. https://doi.org/10.4049/jimmunol.2001413
35. Li R, Sun X, Shu Y, Wang Y, Xiao L, Wang Z, Hu X, Kermode AG and Qiu W. (2017) Serum CCL20 and its association with SIRT1 activity in multiple sclerosis patients. J Neuroimmunol 313:56-60. https://doi.org/10.1016/j.jneuroim.2017.10.013
36. Lindberg RA, Juan TS, Welcher AA, Sun Y, Cupples R, Guthrie B and Fletcher FA. (1998) Cloning and characterization of a specific receptor for mouse oncostatin M. Mol Cell Biol 18(6):3357-67. https://doi.org/10.1128/mcb.18.6.3357
37. Liston A, Kohler RE, Townley S, Haylock-Jacobs S, Comerford I, Caon AC, Webster J, Harrison JM, Swann J, Clark-Lewis I, Korner H and McColl SR. (2009) Inhibition of CCR6 function reduces the severity of experimental

autoimmune encephalomyelitis via effects on the priming phase of the immune response. J Immunol 182(5):3121-30. https://doi.org/10.4049/jimmunol.0713169
38. Lopes Pinheiro MA, Kooij G, Mizee MR, Kamermans A, Enzmann G, Lyck R, Schwaninger M, Engelhardt B and de Vries HE. (2016) Immune cell trafficking across the barriers of the central nervous system in multiple sclerosis and stroke. Biochim Biophys Acta 1862(3):461-71. https://doi.org/10.1016/j.bbadis.2015.10.018
39. Ma Q, Shimaoka M, Lu C, Jing H, Carman CV and Springer TA. (2002) Activation-induced conformational changes in the I domain region of lymphocyte function-associated antigen 1. J Biol Chem 277(12):10638-41. https://doi.org/10.1074/jbc.M112417200
40. Maki W, Morales RE, Carroll VA, Telford WG, Knibbs RN, Stoolman LM and Hwang ST. (2002) CCR6 colocalizes with CD18 and enhances adhesion to activated endothelial cells in CCR6-transduced Jurkat T cells. J Immunol 169(5):2346-53. https://doi.org/10.4049/jimmunol.169.5.2346
41. Marchetti L and Engelhardt B. (2020) Immune cell trafficking across the blood-brain barrier in the absence and presence of neuroinflammation. Vasc Biol 2(1):H1-h18. https://doi.org/10.1530/vb-19-0033
42. Meares GP, Ma X, Qin H and Benveniste EN. (2012) Regulation of CCL20 expression in astrocytes by IL-6 and IL-17. Glia 60(5):771-81. https://doi.org/10.1002/glia.22307
43. Michel L, Grasmuck C, Charabati M, Lécuyer MA, Zandee S, Dhaeze T, Alvarez JI, Li R, Larouche S, Bourbonnière L, Moumdjian R, Bouthillier A, Lahav B, Duquette P, Bar-Or A, Gommerman JL, Peelen E and Prat A. (2019) Activated leukocyte cell adhesion molecule regulates B lymphocyte migration across central nervous system barriers. Sci Transl Med 11(518). https://doi.org/10.1126/scitranslmed.aaw0475
44. Moidunny S, Dias RB, Wesseling E, Sekino Y, Boddeke HW, Sebastião AM and Biber K. (2010) Interleukin-6-type cytokines in neuroprotection and neuromodulation: oncostatin M, but not leukemia inhibitory factor, requires neuronal adenosine A1 receptor function. J Neurochem 114(6):1667-77. https://doi.org/10.1111/j.1471-4159.2010.06881.x
45. Mony JT, Khorooshi R and Owens T. (2014) Chemokine receptor expression by inflammatory T cells in EAE. Front Cell Neurosci 8:187. https://doi.org/10.3389/fncel.2014.00187
46. Moser T, Akgün K, Proschmann U, Sellner J and Ziemssen T. (2020) The role of TH17 cells in multiple sclerosis: Therapeutic implications. Autoimmun Rev 19(10):102647. https://doi.org/10.1016/j.autrev.2020.102647
47. Murakami M, Kamimura D and Hirano T. (2019) Pleiotropy and Specificity: Insights from the Interleukin 6 Family of Cytokines. Immunity 50(4):812-31. https://doi.org/10.1016/j.immuni.2019.03.027
48. Nakamura K, Nonaka H, Saito H, Tanaka M and Miyajima A. (2004) Hepatocyte proliferation and tissue remodeling is impaired after liver injury in oncostatin M receptor knockout mice. Hepatology 39(3):635-44. https://doi.org/10.1002/hep.20086
49. Profaci CP, Munji RN, Pulido RS and Daneman R. (2020) The blood-brain barrier in health and disease: Important unanswered questions. J Exp Med 217(4). https://doi.org/10.1084/jem.20190062
50. Reboldi A, Coisne C, Baumjohann D, Benvenuto F, Bottinelli D, Lira S, Uccelli A, Lanzavecchia A, Engelhardt B and Sallusto F. (2009) C-C chemokine receptor 6-regulated entry of TH-17 cells into the CNS through the choroid plexus is required for the initiation of EAE. Nat Immunol 10(5):514-23. https://doi.org/10.1038/ni.1716
51. Repovic P and Benveniste EN. (2002) Prostaglandin E2 is a novel inducer of oncostatin-M expression in macrophages and microglia. J Neurosci 22(13):5334-43. https://doi.org/10.1523/jneurosci.22-13-05334.2002
52. Rodríguez-Lorenzo S, Ferreira Francisco DM, Vos R, van Het Hof B, Rijnsburger M, Schroten H, Ishikawa H, Beaino W, Bruggmann R, Kooij G and de Vries HE. (2020) Altered secretory and neuroprotective function of the choroid plexus in progressive multiple sclerosis. Acta Neuropathol Commun 8(1):35. https://doi.org/10.1186/s40478-020-00903-y
53. Ruprecht K, Kuhlmann T, Seif F, Hummel V, Kruse N, Brück W and Rieckmann P. (2001) Effects of oncostatin M on human cerebral endothelial cells and expression in inflammatory brain lesions. J Neuropathol Exp Neurol 60(11):1087-98. https://doi.org/10.1093/jnen/60.11.1087
54. Sambrano J, Chigaev A, Nichani KS, Smagley Y, Sklar LA and Houston JP. (2018) Evaluating integrin activation with time-resolved flow cytometry. J Biomed Opt 23(7):1-10. https://doi.org/10.1117/1.Jbo.23.7.075004
55. Slaets H, Nelissen S, Janssens K, Vidal PM, Lemmens E, Stinissen P, Hendrix S and Hellings N. (2014) Oncostatin M reduces lesion size and promotes functional recovery and neurite outgrowth after spinal cord injury. Mol Neurobiol 50(3):1142-51. https://doi.org/10.1007/s12035-014-8795-5
56. Srinivasan B, Kolli AR, Esch MB, Abaci HE, Shuler ML and Hickman JJ. (2015) TEER measurement techniques for in vitro barrier model systems. J Lab Autom 20(2):107-26. https://doi.org/10.1177/2211068214561025

57. Sugaya M, Fang L, Cardones AR, Kakinuma T, Jaber SH, Blauvelt A and Hwang ST. (2006) Oncostatin M enhances CCL21 expression by microvascular endothelial cells and increases the efficiency of dendritic cell trafficking to lymph nodes. J Immunol 177(11):7665-72. https://doi.org/10.4049/jimmunol.177.11.7665
58. Takata F, Dohgu S, Matsumoto J, Machida T, Sakaguchi S, Kimura I, Yamauchi A and Kataoka Y. (2018) Oncostatin M-induced blood-brain barrier impairment is due to prolonged activation of STAT3 signaling in vitro. J Cell Biochem 119(11):9055-63. https://doi.org/10.1002/jcb.27162
59. Takata F, Dohgu S, Sakaguchi S, Sakai K, Yamanaka G, Iwao T, Matsumoto J, Kimura I, Sezaki Y, Tanaka Y, Yamauchi A and Kataoka Y. (2019) Oncostatin-M-Reactive Pericytes Aggravate Blood-Brain Barrier Dysfunction by Activating JAK/STAT3 Signaling In Vitro. Neuroscience 422:12-20. https://doi.org/10.1016/j.neuroscience.2019.10.014
60. Takata F, Sumi N, Nishioku T, Harada E, Wakigawa T, Shuto H, Yamauchi A and Kataoka Y. (2008) Oncostatin M induces functional and structural impairment of blood-brain barriers comprised of rat brain capillary endothelial cells. Neurosci Lett 441(2):163-6. https://doi.org/10.1016/j.neulet.2008.06.030
61. Tanaka M, Hirabayashi Y, Sekiguchi T, Inoue T, Katsuki M and Miyajima A. (2003) Targeted disruption of oncostatin M receptor results in altered hematopoiesis. Blood 102(9):3154-62. https://doi.org/10.1182/blood-2003-02-0367
62. Tenenbaum T, Steinmann U, Friedrich C, Berger J, Schwerk C and Schroten H. (2013) Culture models to study leukocyte trafficking across the choroid plexus. Fluids Barriers CNS 10(1):1. https://doi.org/10.1186/2045-8118-10-1
63. Tinevez JY, Perry N, Schindelin J, Hoopes GM, Reynolds GD, Laplantine E, Bednarek SY, Shorte SL and Eliceiri KW. (2017) TrackMate: An open and extensible platform for single-particle tracking. Methods 115:80-90. https://doi.org/10.1016/j.ymeth.2016.09.016
64. Ujlaky-Nagy L, Nagy P, Szöllősi J and Vereb G. (2018) Flow Cytometric FRET Analysis of Protein Interactions. Methods Mol Biol 1678:393-419. https://doi.org/10.1007/978-1-4939-7346-0_17
65. van Keulen D, Pouwer MG, Pasterkamp G, van Gool AJ, Sollewijn Gelpke MD, Princen HMG and Tempel D. (2018) Inflammatory cytokine oncostatin M induces endothelial activation in macro- and microvascular endothelial cells and in APOE*3Leiden.CETP mice. PLoS One 13(10):e0204911. https://doi.org/10.1371/journal.pone.0204911
66. Villares R, Cadenas V, Lozano M, Almonacid L, Zaballos A, Martínez AC and Varona R. (2009) CCR6 regulates EAE pathogenesis by controlling regulatory CD4+ T-cell recruitment to target tissues. Eur J Immunol 39(6):1671-81. https://doi.org/10.1002/eji.200839123
67. Walling BL and Kim M. (2018) LFA-1 in T Cell Migration and Differentiation. Front Immunol 9:952. https://doi.org/10.3389/fimmu.2018.00952
68. Weiss TW, Samson AL, Niego B, Daniel PB and Medcalf RL. (2006) Oncostatin M is a neuroprotective cytokine that inhibits excitotoxic injury in vitro and in vivo. Faseb j 20(13):2369-71. https://doi.org/10.1096/fj.06-5850fje
69. Weksler B, Romero IA and Couraud PO. (2013) The hCMEC/D3 cell line as a model of the human blood brain barrier. Fluids Barriers CNS 10(1):16. https://doi.org/10.1186/2045-8118-10-16
70. Wojkowska DW, Szpakowski P and Glabinski A. (2017) Interleukin 17A Promotes Lymphocytes Adhesion and Induces CCL2 and CXCL1 Release from Brain Endothelial Cells. Int J Mol Sci 18(5). https://doi.org/10.3390/ijms18051000
71. Zhang X, Li J, Qin JJ, Cheng WL, Zhu X, Gong FH, She Z, Huang Z, Xia H and Li H. (2017) Oncostatin M receptor β deficiency attenuates atherogenesis by inhibiting JAK2/STAT3 signaling in macrophages. J Lipid Res 58(5):895-906. https://doi.org/10.1194/jlr.M074112